

Discrete Conformal Deformation: Algorithm and Experiments*

Jian Sun[†], Tianqi Wu[‡], Xianfeng Gu[§], and Feng Luo[¶]

Abstract. In this paper, we introduce the definition of discrete conformality for triangulated surfaces with flat cone metrics and describe an algorithm for solving the problem of prescribing curvature, which is to deform the metric discrete conformally so that the curvature of the resulting metric coincides with the prescribed curvature. We explicitly construct a discrete conformal map between the input triangulated surface and the deformed triangulated surface. Our algorithm can handle a surface with any topology, with or without boundary, and can find a deformed metric for any prescribed curvature satisfying the Gauss–Bonnet formula. In addition, we present the numerical examples to show the convergence of our discrete conformality and to demonstrate the efficiency and the robustness of our algorithm.

Key words. discrete conformal geometry, combinatorial Yamabe flow, diagonal switch, Delaunay triangulation

AMS subject classification. 52C26

DOI. 10.1137/141001986

1. Introduction. In this paper, we introduce a definition of discrete conformality for triangle meshes and describe an algorithm for solving the problem of prescribing curvature, which is to deform the metric discrete conformally so that the curvature of the resulting metric coincides with the prescribed curvature. In addition, we explicitly construct a discrete conformal map between the original triangle mesh and the deformed triangle mesh. The problem of prescribing curvature has many applications in various engineering fields, including computer vision, image processing, and computer graphics. For instance, by setting the curvature to be zero, one can discrete conformally flatten a triangle mesh into the plane and thus obtain a discrete conformal parametrization of the mesh.

Our discrete conformal deformation consists of two basic operations: *vertex scaling* and *cocircular diagonal switch* (see Figure 1). Assume a closed surface S is equipped with a triangulation $T = (V, E, F)$, where V , E , and F are the vertex set, the edge set, and the triangle set, respectively. An edge length assignment $l : E \rightarrow \mathbb{R}^+$ assigns any edge $e \in E$ the length $l(e)$, which determines a metric on S , provided that the triangle inequalities are

*Received by the editors December 30, 2014; accepted for publication April 21, 2015; published electronically July 14, 2015. The work of the first and second authors was partially supported by the NSF of China (grants 11371220 and 1127101).

<http://www.siam.org/journals/siims/8-3/100198.html>

[†]Mathematical Sciences Center, Tsinghua University, Beijing 100084, China (jsun@math.tsinghua.edu.cn).

[‡]Courant Institute of the Mathematical Sciences, New York University, New York, NY 10012 (tianqi@cims.nyu.edu). This work was done while this author was at Tsinghua University.

[§]Department of Computer Science, Stony Brook University, New York, NY 11794 (gu@cs.stonybrook.edu). The work of this author was partially supported by the NSF (grants DMS-1418255 and DMS-1221339) and by AFOSR (grant FA9550-10-1-0294).

[¶]Department of Mathematics, Rutgers University, New Brunswick, NJ 08854 (fluo@math.rutgers.edu). The work of this author was partially supported by the NSF (grants DMS 1222663, DMS 1207832, and DMS 1405106).

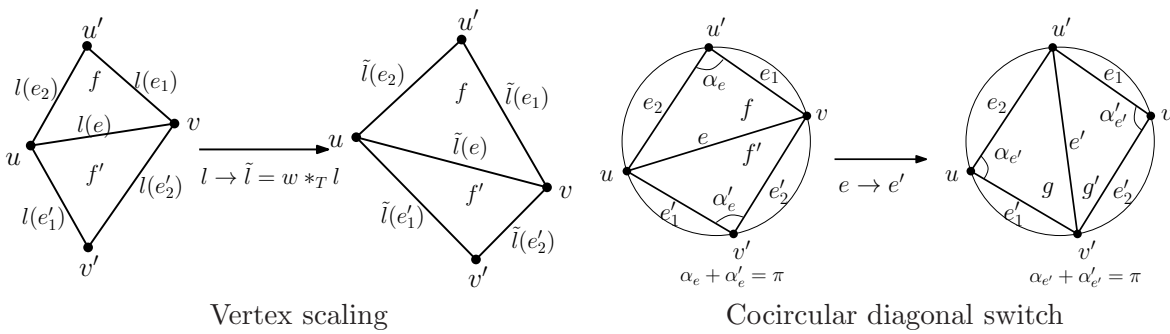


Figure 1. Two basic operations in discrete conformal deformation.

satisfied for all triangles in T . Vertex scaling is a special way of changing the edge lengths. Specifically, the vertex scaling of the edge length assignment l by a function $w : V \rightarrow \mathbb{R}$ is another edge length assignment, denoted $w *_T l$, so that for any edge $e \in E$ with the endpoints $u, v \in V$,

$$(1.1) \quad w *_T l(e) = e^{w(u)+w(v)} l(e).$$

We call the function w the discrete conformal factor. A discrete conformal factor w is legitimate if the edge length assignment $w *_T l$ satisfies the triangle inequalities for all the triangles in T . By a simple dimension counting, the vertex scalings of l will not in general cover all possible edge length assignments on E . For an edge e in T , denote by f and f' the two triangles in T incident to e , and e_1, e_2 , respectively, e'_1, e'_2 , are two other edges of f , respectively, f' , listed counterclockwise, as shown in Figure 1. Define the length cross ratio of the edge e under the edge length assignment l as $c_l(e) = (l(e_1)l(e'_1))/(l(e_2)l(e'_2))$. Then it is easy to verify that an edge length assignment \tilde{l} is a vertex scaling of l if and only if the length cross ratio is preserved, i.e., $c_l(e) = c_{\tilde{l}}(e)$ for any edge e in T .

The vertex scaling operation was introduced by Roček and Williams in physics [33] and independently by Luo in mathematics [29]. Luo established a (convex) variational principle associated to vertex scaling. This variational principle has many nice properties. The one most relevant to the applications in engineering fields is that there is an efficient algorithm to solve the problem of prescribing curvature, and thus the problem of discrete conformal parametrization as a special case. The main observation is that, given a triangulation T and an edge length assignment l over its edges E , the conformal factor w such that the metric determined by $w *_T l$ achieves the prescribed curvature is the unique minimizer of a convex energy, whose gradient and Hessian can be explicitly estimated. Thus, the minimizer can be efficiently computed by Newton's method. The convex energy discovered by Luo [29] takes the form of a path integral of a differential one-form. An explicit formula of this convex energy based on the Lobachevsky function was found later by Springborn, Schröder, and Pinkall [35]. However, there are the cases where the discrete conformal factor w solving the prescribing curvature problem does not exist. In fact, in those cases, the minimizer w of the above convex energy is not legitimate.

To tackle the issue of existence, we introduce the second operation: diagonal switch. Let e be an edge in T adjacent to two distinct triangles f and f' in T ; the diagonal switch of

the edge e replaces e by the other diagonal e' of the quadrilateral $f \cup f'$. This also replaces the triangles f, f' by two new triangles, g, g' , as shown in Figure 1, and produces a new triangulation $T' = (V, E', F')$ on S . With diagonal switch, we can extend the domain of legitimate discrete conformal factors. To see this, we start with a Euclidean triangulation T and an initial edge length assignment l over the edges in T , and then we vertex scale l by continuously changing the function w along the gradient of the above convex energy. At some point, some triangle in T may become degenerate under the new edge length assignment $w * l$, that is, the triangle inequality becomes an equality. It was shown by Luo [29] that in any degenerated triangle one of its inner angles must equal π . By diagonally switching the edge opposite to that angle, the degenerated triangle is removed. In this way, one may make the conformal factor w legitimate. However, diagonal switch brings up many complicated issues. For instance, with diagonal switch, a priori, the energy depends on not only the discrete conformal factor w , but also the triangulations on S , which are combinatorial structures. *Can the energy with combinatorial variables still be convex?* In addition, new edges are emerging with diagonal switches. *What is the assignment of the lengths for these edges which are not in the initial triangulation?* Furthermore, *if multiple triangles simultaneously become degenerate, do different sequences of diagonal switches lead to the same solution?*

Our key observation to make diagonal switch work nicely is to switch an edge well before its incident triangles become degenerate. Specifically, an edge $e \in E$ shared by the triangles f, f' is switched when it fails to be Delaunay, that is, the sum of the angles opposite to e in f and f' becomes bigger than π . We call it cocircular diagonal switch, as the edge e is switched at the moment that the quadrilateral $f \cup f'$ become cocircular. See Figure 1. We will answer the above three questions later. Roughly speaking, two polyhedral (PL) metrics on S are discrete conformal if one can be deformed to the other by a sequence of vertex scalings and cocircular diagonal switches. The rigorous definition is given in Definition 3.1. Based on this discrete conformality, there always exists a PL metric which is discrete conformal to the initial PL metric and achieves any prescribed curvature. Furthermore, such a metric can be computed using an efficient algorithm through minimizing a convex energy. The algorithm can handle surfaces with any topology with or without boundary.

In this paper, we describe our theory of discrete conformality with a focus on explaining the algorithm for solving the problem of prescribing curvature, and we present the numerical examples, in particular showing the convergence of our discrete conformality. For the rigorous mathematical treatment of our theory, interested readers are referred to [15, 14].

Related work. There has been a lot of research into discrete conformality, and we will not attempt a comprehensive review here. Instead, we focus on methods closely related to ours. Note that all previous work deals with the concept of discrete conformality with fixed triangulations.

Bobenko, Pinkall, and Springborn [4] introduced a geometric interpretation to vertex scaling in both Euclidean and hyperbolic geometry using the volume of generalized hyperbolic tetrahedron. Glickenstein [11, 12] extended vertex scaling to 3-dimensional piecewise flat manifolds.

One closely related work is circle patterns, where a system of circles is associated with vertices. Two triangulated surfaces are considered conformally equivalent if the intersection

angles of the circles are equal in both triangulated surfaces. The idea of approaching discrete conformality through circle patterns goes back to Thurston (see [36]). Rodin and Sullivan [34] proved Thurston's conjecture that Riemann mapping can be approximated by tangential circle packings (i.e., circle patterns with 0 intersection angles) of hexagonal triangulations, and He and Schramm [20] later showed the convergence is C^∞ . Colin de Verdière [8] discovered a variational principle for circle patterns with intersection angles in $[0, \pi/2]$, and Chow and Luo [7] introduced discrete Ricci flow based on circle packing and established a convergence theorem. An issue with circle patterns is that not all metrics can be realized by circle patterns with intersection angles in $[0, \pi/2]$. To tackle this issue, Bowers and Stephenson [6] introduced inversive circle patterns where circles do not necessarily intersect. Guo [18] established a variational principle for inversive circle patterns and showed that inversive distance circle patterns are locally rigid, i.e., locally determined by the curvature. Luo gave a proof for global rigidity in [30]. However, the question of existence to the problem of prescribing curvature remains open. It is interesting to see if diagonal switch can help solving the existence problem. Many practical algorithms based on circle patterns have been proposed for conformally flattening triangulated surfaces, including [25, 24].

Conformality is closely related to harmonicity. Pinkall and Polthier [31] proposed an approach for flattening a triangulated surface by computing a pair of discrete harmonic functions conjugate to each other. Gu and Yau [16] proposed a method to conformally flatten a surface into the plane using holomorphic one-forms. Assuming $h = f(z)dz$ is a holomorphic one-form of the surface, the metric $|f(z)|^2 dz d\bar{z}$ is then conformal and flat when $f(z) \neq 0$. Noticing that any holomorphic one-form can be decomposed as $h = \omega + i(*\omega)$, where ω is a real harmonic one-form and $*\omega$ is its conjugate, Gu and Yau developed discrete algorithms to approximate holomorphic one-forms from a triangulated surface by computing discrete harmonic one-forms and their conjugates.

Another class of methods achieves conformality by minimizing conformal distortion. In these methods, piecewise linear maps are used to approximate actual conformal maps. Noticing that $h_{\bar{z}} = 0$ for a conformal map h , Levy et al. [26] proposed a method for finding a piecewise linear map f from a triangulated surface into the plane by minimizing $\|f_{\bar{z}}\|_{L_2}$. Lipman [27] proposed a method for finding a piecewise linear map f whose conformal distortion $\frac{|f_z| + |f_{\bar{z}}|}{|f_z| - |f_{\bar{z}}|}$ is bounded. Lui et al. [28] noticed that the magnitude of the Beltrami coefficient $\mu = \frac{h_{\bar{z}}}{h_z}$ is constant for the extremal map h (the map with minimal conformal distortion) and proposed an iterative procedure to find a piecewise linear map f whose Beltrami coefficient has constant magnitude.

With our new definition of discrete conformality, we establish a discrete uniformization theorem. In a series of papers on developing discrete uniformization theorem [23, 22, 21], Hersensky proved several important theorems based on discrete harmonic maps and cellular decompositions. His approach is complementary to our work.

2. PL metrics and triangulations. The purpose of this section is to explain the relation between PL metrics and triangulations and to familiarize the readers with a more general triangulated surface than is usually encountered in many engineering fields with simplicial complex structure (i.e., any higher dimensional simplex is uniquely determined by its vertices). For simplicity, we assume the surface S is closed without boundary. We will discuss how to

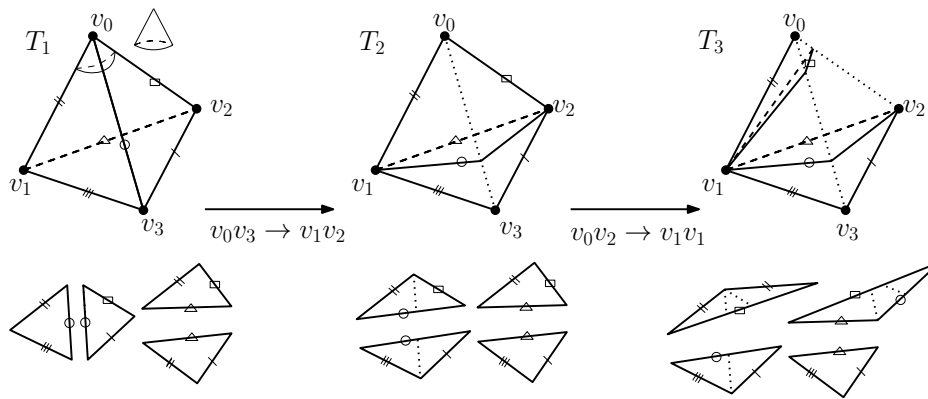


Figure 2. Triangulations of the boundary of a tetrahedron. The second row shows the gluing pattern of the triangles for different triangulations, where the edges marked with the same symbol are glued together. The triangulation T_2 (T_3) is obtained by switching an edge in T_1 (T_2).

deal with surfaces with boundaries in section 3.1.

We start with a triangulated surface S with which we are familiar, i.e., embedded in \mathbb{R}^3 where each triangle is the convex hull of its three vertices. For example, the boundary of a tetrahedron in \mathbb{R}^3 is such a triangle mesh with four Euclidean triangles, as shown in the leftmost picture in Figure 2. Denote by V the set of vertices. Note that, other than the vertices, any point $p \in S$ has a flat neighborhood. This is obvious if p is in the interior of a triangle which is Euclidean. For p in the interior of an edge, one can flatten the two triangles incident to the edge into the Euclidean plane, and thus p also has an (intrinsically) flat neighborhood. For a vertex $v \in V$, it has a neighborhood like a cone, as shown in Figure 2. Thus the metric on S is flat with possible cone singularities at a discrete set of vertices. We call such a metric a *polyhedral metric*, or simply PL metric. In general, a surface with a PL metric is obtained by isometrically gluing pairs of edges of a finite collection of Euclidean triangles. See Figure 2 for examples. The converse also holds; that is, any surface with a PL metric can be partitioned into Euclidean triangles. In fact, this can be done by keeping connecting pairs of cone singular vertices with intrinsically straight edges on S until no edge can be added without intersecting the previously added edges in their interiors. Each partition is in fact a triangulation with Euclidean triangles (in short, *Euclidean triangulation*) on the surface S . The curvature of a PL metric is 0 everywhere except at the cone singular vertices where the curvature is defined as 2π less the cone angle. Given a Euclidean triangulation $T = (V, E, F)$ on the surface S , one can evaluate the cone angle at a vertex v by summing the inner angles at v in the triangulation T , and even deform the PL metric d by changing the edge length. For an edge $e \in E$, let $d(e)$ be the length of e measured in the metric d . The edge length assignment $l : E \rightarrow \mathbb{R}^+$ with $l(e) = d(e)$ uniquely determines the PL metric d .

Given a PL metric d on S , there may be more than one Euclidean triangulation. Figure 2 shows three different triangulations of the boundary of a tetrahedron, where the triangulation T_2 , respectively, T_3 , is obtained by diagonally switching the edge v_0v_3 in T_1 , respectively, the edge v_0v_2 in T_2 . It is generally true that any two (Euclidean) triangulations on S with the same set of vertices V are related by diagonal switches [19]. Among those Euclidean

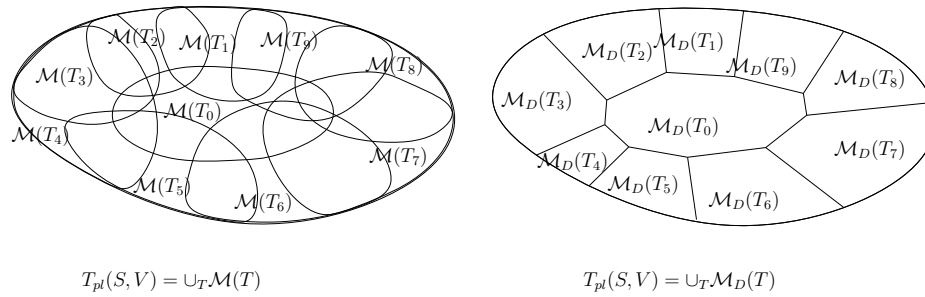


Figure 3. Coverings of the space of PL metrics $T_{pl}(S, V)$.

triangulations, there always exists a Delaunay triangulation where every edge is Delaunay; that is, the sum of the angles opposite the edge is no bigger than π [5]. There may exist more than one Delaunay triangulation. If it happens that the sum of the angles opposite an edge is exactly π , then by (cocircular) diagonally switching that edge, we obtain another Delaunay triangulation. In fact, any two Delaunay triangulations are related by a sequence of cocircular diagonal switches.

In this paper, we fix the topology of the closed surface S and a finite nonempty set $V \subset S$ and call the pair (S, V) a *marked surface*. A PL metric on the pair (S, V) is a PL metric on S with the cone singularities in V ; the curvature of a PL metric on (S, V) is the function $K : V \rightarrow \mathbb{R}$ sending a vertex v to 2π less than the cone angle at v ; and a triangulation of the pair (S, V) is a triangulation on S with vertex set V . The curvature K of a PL metric satisfies the Gauss–Bonnet formula: $\sum_{v \in V} K(v) = 2\pi\chi(S)$, where $\chi(S)$ is the Euler characteristic number of S . If $T = (V, E, F)$ is a triangulation on (S, V) , then $\chi(S) = |V| - |E| + |F|$.

Let $T_{pl}(S, V)$ be the space of PL metrics on (S, V) .¹ Given a triangulation T of (S, V) with set of edges $E = E(T)$, let $\mathcal{E}(T)$ be the set of edge length assignments so that the triangle inequalities are satisfied for all triangles in T . $\mathcal{E}(T)$ is a convex polytope in $\mathbb{R}^{|E(T)|}$. Since any edge length assignment $l \in \mathcal{E}(T)$ determines a PL metric d on (S, V) with $d(e) = l(e)$, there is an injective map

$$(2.1) \quad \Phi_T : \mathcal{E}(T) \rightarrow T_{pl}(S, V)$$

sending l to a PL metric $d_l = \Phi_T(l)$ on (S, V) . The image $\mathcal{M}(T) := \Phi_T(\mathcal{E}(T))$ is the space of all PL metrics d on (S, V) for which T is a Euclidean triangulation in d . From the previous discussion, for any PL metric d on (S, V) , there exists a Euclidean triangulation T on (S, V) whose edge length assignment is given by the metric d ; i.e., there exists an edge length assignment $l \in \mathcal{E}(T)$ with $d = \Phi_T(l)$. Thus we have $T_{pl}(S, V) = \cup_T \mathcal{M}(T)$, where the union is over all triangulations on (S, V) . Notice that $E(T) = (-3\chi(S) + 3|V|)$, where $\chi(S)$ is the Euler characteristic number of S , which is independent of T . This means that $T_{pl}(S, V)$ is a manifold of dimension $(-3\chi(S) + 3|V|)$ with coordinate charts $\{(\mathcal{M}(T), \Phi_T^{-1}) | T \text{ is a triangulation on } (S, V)\}$, as illustrated in Figure 3. Note that in general $T_{pl}(S, V) \neq \mathcal{M}(T)$.

¹Strictly speaking, we should consider the set of equivalence classes of PL metrics where two PL metrics d, d' on (S, V) are equivalent if there is an isometry $h : (S, V, d) \rightarrow (S, V, d')$ that is homotopic to the identity map on (S, V) . However, this difference is subtle and can be ignored, especially for the purpose of understanding the algorithm.

Now we consider a subset of $\mathcal{E}(T)$:

$$(2.2) \quad \mathcal{E}_D(T) = \{l \in \mathcal{E}(T) \mid T \text{ is a Delaunay triangulation on } (S, V) \text{ in the PL metric } \Phi_T(l)\}.$$

As we discussed before, for any PL metric d , there is a Delaunay triangulation T whose edge length assignment l is given by the metric d , i.e., $d = \Phi_T(l)$. Thus the set $\{\mathcal{E}_D(T) \mid T \text{ is a triangulation on } (S, V)\}$ also covers $T_{pl}(S, V)$. In fact, this set forms a cell decomposition of $T_{pl}(S, V)$ [32, 15], as illustrated in Figure 3. Thus one may say that Delaunay triangulation is canonical as it is uniquely determined by the PL metric except for those metrics on the cell boundary which have multiple Delaunay triangulations.

Finally, we remark that in a Euclidean triangulation T on (S, V) , it is possible to have multiple intrinsically straight edges between two vertices (e.g., the edges marked “o” and “ Δ ” between v_1 and v_2 in the triangulation T_2 in Figure 2), and even to have an intrinsically straight loop edge (e.g., the edge marked “ \square ” in the triangulation T_3 in Figure 2). Note that even if we start with a mesh with simplicial complex structure, we may end up with a mesh with a more general structure than that above, as we allow diagonal switches.

3. Discrete conformality. Now we are ready to present our definition of discrete conformality.

Definition 3.1 (discrete conformality for surfaces without boundary). *Two PL metrics d, d' on (S, V) are discrete conformal if there exist sequences of PL metrics $d_0 = d, \dots, d_m = d'$ on (S, V) and triangulations $\mathcal{T}_0, \dots, \mathcal{T}_m$ of (S, V) satisfying the following:*

- (a) *Each \mathcal{T}_i is Delaunay in d_i .*
- (b) *If $\mathcal{T}_i = \mathcal{T}_{i+1}$, then $l_{i+1} = w *_{\mathcal{T}_i} l_i$ for a conformal factor $w : V \rightarrow \mathbb{R}$, where l_{i+1} and l_i are the edge length assignments over the edges of \mathcal{T}_i with $l_{i+1}(e) = d_{i+1}(e)$ and $l_i(e) = d_i(e)$ for any edge e in \mathcal{T}_i .*
- (c) *If $\mathcal{T}_i \neq \mathcal{T}_{i+1}$, then $d_{i+1} = d_i$,² and $\mathcal{T}_i, \mathcal{T}_{i+1}$ are related by cocircular diagonal switches.*

This definition means that d, d' are discrete conformal if and only if there exists a path connecting two PL metrics in the space of $T_{pl}(S, V)$ such that, within a cell $\mathcal{E}_D(T)$, the metrics deform along the path by vertex scalings, and on the cell boundary the Delaunay triangulation is changed to another via cocircular diagonal switches.

Condition (a) in the definition is crucial. Note that vertex scaling depends on the choice of triangulations. The vertex scaling of the same PL metric but under different Euclidean triangulations may generate different PL metrics. So the previous definition of discrete conformality by vertex scaling [33, 29, 4] heavily depends on the triangulations, which is not inherent to PL metrics. On the other hand, by restricting it to Delaunay triangulations which are canonical to PL metrics, our definition of discrete conformality is inherent to PL metrics. With this definition, we are able to prove the following uniformization theorem in [15].

Theorem 3.2. *Suppose (S, V) is a closed connected marked surface and d is any PL metric on (S, V) . Then for any $K^* : V \rightarrow (-\infty, 2\pi)$ with $\sum_{v \in V} K^*(v) = 2\pi\chi(S)$, there exists a PL metric d' , unique up to scaling, on (S, V) such that d' is discrete conformal to d and the discrete curvature of d' is K^* .*

²Strictly speaking, $d_{i+1} = d_i$ in the sense of equivalence class; that is, (S, d_i) is isometric to (S, d_{i+1}) by an isometry homotopic to the identity in (S, V) .

In the above theorem, the conditions on the curvature K^* are necessary for K^* to be a curvature of a PL metric on (S, V) . The theorem states that those conditions are also sufficient for K^* to be achieved by a metric that is discrete conformal to the given metric d . This solves the existence and the uniqueness of the discrete conformal deformation mentioned in the introduction.

3.1. Surfaces with boundary. To deal with a surface with boundary, our strategy is to double the surface to remove the boundary, that is, make another copy of the original surface and glue them along the boundary, to apply the discrete conformal deformation described above to the doubled surface, and finally to cut out a copy of the deformed surface from the deformed doubled surface.

Let B be the boundary of the marked surface (S, V) . Given a PL metric d on S , B consists of a set of closed polygonal loops. A Euclidean triangulation on (S, V) is a partition of S into Euclidean triangles with the vertices V . Note that those edges of the polygonal loops of B have to be in the triangulation. For a vertex $v \in V$ on the boundary, its curvature is defined as π less than the cone angle at v . With this definition, the Gauss–Bonnet theorem still holds: $\sum_{v \in V} K(v) = 2\pi\chi(S)$.

The doubled surface of (S, V) is defined by taking the disjoint union of two copies of (S, V) and identifying the points on the boundary by a homeomorphism $f : B \rightarrow B$ which preserves the vertices on the boundary. Denote by (\tilde{S}, \tilde{V}) the doubled surface of (S, V) . A PL metric d on (S, V) induces a PL metric \tilde{d} on (\tilde{S}, \tilde{V}) by forcing the gluing map f to be isometric in d . We call \tilde{d} the doubled metric of d . Conversely, a PL metric on the doubled surface (\tilde{S}, \tilde{V}) is said to respect the doubling structure if it is the doubled metric of a PL metric on (S, V) . Let the map $h : (\tilde{S}, \tilde{V}) \rightarrow (\tilde{S}, \tilde{V})$ be the mirror map sending a point to the other copy. The map h is a self-isometric map if the PL metric on (\tilde{S}, \tilde{V}) respects the doubling structure. For convenience, the set of fixed points of the map h is called the boundary of (\tilde{S}, \tilde{V}) .

Definition 3.3 (discrete conformality for surfaces with boundary). *Two PL metrics d, d' on the surface (S, V) with boundary are discrete conformal if their doubled metrics on the doubled surface of (S, V) are discrete conformal according to Definition 3.1.*

Theorem 3.4. *Suppose (S, V) is a connected marked surface with boundary and d is any PL metric on (S, V) . Then for any $K^* : V \rightarrow (-\infty, 2\pi)$ with $\sum_{v \in V} K^*(v) = 2\pi\chi(S)$ and $K^*(v) < \pi$ for a vertex v on the boundary, there exists a PL metric d' , unique up to scaling, on the surface (S, V) such that d' is discrete conformal to d and the discrete curvature of d' is the prescribed curvature K^* .*

The proof of the above theorem is deferred to the appendix. The basic idea is as follows. We obtain the doubled surface (\tilde{S}, \tilde{V}) and prescribe the curvature $\tilde{K}^*(v)$ for (\tilde{S}, \tilde{V}) as follows: for a vertex v on the boundary, set $\tilde{K}^*(v) = 2 * K^*(v)$, and for a vertex in the interior, set $\tilde{K}^*(v) = K^*(v)$. It is easy to verify that the curvature \tilde{K}^* satisfies the hypotheses imposed in Theorem 3.2 to a target curvature on (\tilde{S}, \tilde{V}) . Thus there exists a PL metric \tilde{d}' discrete conformal to \tilde{d} , and the discrete curvature of \tilde{d}' is the curvature of \tilde{K}^* . It remains to show that \tilde{d}' respects the doubling structure, and the restriction of \tilde{d}' onto S is the PL metric d' with the property stated in the theorem. The key is to show that the conformal factor w continues to respect the conformal structure, i.e., $w(h(v)) = w(v)$, and the Delaunay triangulation T of (\tilde{S}, \tilde{V}) under metric \tilde{d}' has a certain symmetric property. Specifically, any triangle f crossing

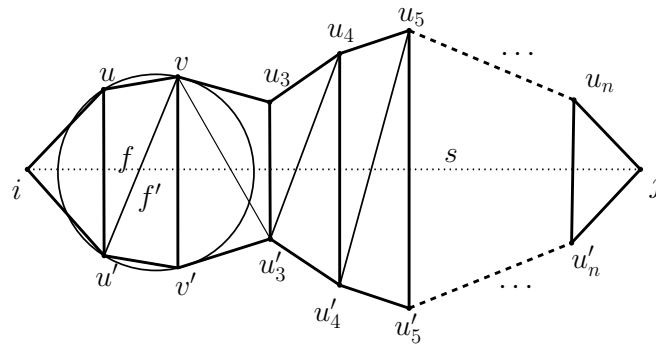


Figure 4. The symmetric property of the triangles crossing an edge ij on the boundary.

an edge ij on the boundary has to have two vertices u, u' so that $u' = h(u)$, and, moreover, if the third vertex v of the triangle f is neither i nor j , the neighboring triangle $f' = v'vu'$ with $v' = h(v)$ must also cross the edge ij , and two triangles f and f' form a cocircular quadrilateral, as shown in Figure 4. In addition, the boundary edge ij remains straight after the discrete conformal deformation, and they subdivide the crossed cocircular quadrilaterals into two identical pieces. This makes it easy to algorithmically cut out a copy of the deformed surface from the deformed doubled surface.

4. Convex energy. In this section, we describe a convex energy for solving the problem of prescribing curvature. This will answer the first question raised in the introduction positively; i.e., there is still a convex energy even with the seeming appearance of combinatorial variables for changing triangulations. Roughly speaking, as our discrete conformality only involves Delaunay triangulations, which are canonical and determined by PL metrics, the combinatorial variables of triangulations are not independent.

Given a PL metric d on (S, V) , we let $C(d)$ denote the space of PL metrics that are discrete conformal to d . The following lemma about $C(d)$ is important.

Lemma 4.1. *There is a C^1 diffeomorphism from $C(d)$ to $\mathbb{R}^{|V|}$ where a point $w \in \mathbb{R}^{|V|}$ is understood as a discrete conformal factor on V .*

This lemma means there is a one-to-one correspondence between the PL metrics discrete conformal to d and all discrete conformal factors on V . The energy is defined over $\mathbb{R}^{|V|}$, the space of all discrete conformal factors. The rigorous mathematical proof of this lemma uses the Teichmüller theory by establishing a one-to-one correspondence between PL metrics on (S, V) and the hyperbolic metrics on $S \setminus V$ with cusps and decorations at V [15]. In this paper, we will not explain this connection to hyperbolic metrics. Instead, we will give an intuitive explanation of the lemma aiming at an understanding of the algorithmic aspects, which does not, however, mathematically prove it.

The space $C(d) \subset T_{pl}(S, V)$ has a cell decomposition induced by that of $T_{pl}(S, V)$, where a cell is the intersection $C(d) \cap \mathcal{M}_D(T)$ for some triangulation T on (S, V) . Note that the number of cells in $C(d)$ is finite [15]. See Figure 5. Let T_0 be a Delaunay triangulation in the initial PL metric d , and let l_{T_0} be the edge length assignment with $l_{T_0}(e) = d(e)$ for any edge e of T_0 . Given a conformal factor $w \in \mathbb{R}^{|V|}$, let w also denote a path in $\mathbb{R}^{|V|}$ from 0 and w , that is, $w : [0, 1] \rightarrow \mathbb{R}^{|V|}$ with $w(0) = 0$ and $w(1) = w$. We have $l_{T_0} = w(0) *_{T_0} l_{T_0}$.

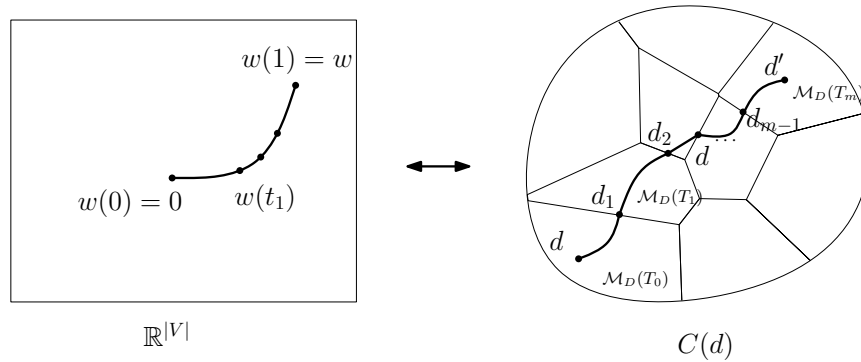


Figure 5. One-to-one correspondence between the conformal factors and the PL metrics on (S, V) discrete conformal to a PL metric d .

As we move along the path w , we continuously deform the PL metric d discrete conformally through vertex scaling l_{T_0} by $w(t)$. This will trace out a path $\Phi_{T_0}(w(t) *_{T_0} l_{T_0})$ in the cell $C(d) \cap \mathcal{M}_D(T_0)$. At some point, this path may hit the boundary of the cell. Assume that happened at $t = t_1$ and, for example, the quadrilateral $f \cup f'$ with the diagonal e becomes cocircular in the metric $d_1 = \Phi_{T_0}(w(t_1) *_{T_0} l_{T_0})$. We diagonal switch the edge e to the edge e' and obtain another Delaunay triangulation T_1 in d_1 , as shown in Figure 1. Note that T_0 is also Delaunay in d_1 . Due to the well-known Ptolemy identity for a cocircular quadrilateral, we have

$$\begin{aligned}
 d_1(e') &= \frac{d_1(e_1)d_1(e'_1) + d_1(e_2)d_1(e'_2)}{d_1(e)} \\
 (4.1) \quad &= \frac{l_{T_0}(e_1)l_{T_0}(e'_1) + l_{T_0}(e_2)l_{T_0}(e'_2)}{l_{T_0}(e)} e^{w(t_1)(u') + w(t_1)(v')},
 \end{aligned}$$

where u' and v' are the endpoints of e' . If we let l_{T_1} be the edge length assignment over the edges of T_1 so that $l_{T_1}(e) = l_{T_0}(e)$ for $e \neq e'$ and

$$(4.2) \quad l_{T_1}(e') = \frac{l_{T_0}(e_1)l_{T_0}(e'_1) + l_{T_0}(e_2)l_{T_0}(e'_2)}{l_{T_0}(e)},$$

then we have $d_1 = \Phi_{T_1}(w(t_1) *_{T_1} l_{T_1})$. Note that $l_{T_1}(e')$ for the new edge e' depends only on l_{T_0} and in particular is independent of the conformal factor $w(t_1)$. This answers the second question raised in the introduction on how to assign the initial edge lengths for the new edges after diagonal switches. Repeat the above procedure as we continuously move along the path w . At the end, we reach a metric $d' = \Phi_{T_m}(w *_{T_m} l_{T_m})$ in the cell $C(d) \cap \mathcal{M}_D(T_m)$ for some triangulation T_m . Mathematically, we can show that the final metric d' is independent of the choice of path; namely, if we choose another path connecting 0 and w and repeat the above procedure, we reach the same metric d' . Thus d' depends only on the initial PL metric d and the conformal factor w . We write $d' = w * d$. Conversely, for any PL metric $d' \in C(d)$, one can find a conformal factor $w \in \mathbb{R}^{|V|}$ such that $d' = w * d$. To see this, from the definition of discrete conformality, there is a path in $C(d)$ connecting d and d' . From the above procedure,

it is easy to trace out a path $w : [0, 1] \rightarrow \mathbb{R}^{|V|}$ starting at 0 so that $w(t) * d$ is the path in $C(d)$ connecting d and d' . This shows that there is a one-to-one correspondence between $\mathbb{R}^{|V|}$ and $C(d)$. This in fact answers the third question raised in the introduction positively, i.e., whether different orders of switching diagonals lead to the same final PL metric.

We follow Luo [29] and define the energy as a path integral of a differential one-form on $\mathbb{R}^{|V|}$. Given a PL metric d on (S, V) , let $K : \mathbb{R}^{|V|} \rightarrow \mathbb{R}^{|V|}$ be the curvature map such that $K(w)$ is the curvature of the PL metric $w * d$ on (S, V) for any conformal factor $w \in \mathbb{R}^{|V|}$. Label the vertices V using $1, 2, \dots, n = |V|$. Let K_i and w_i denote the curvature K and the conformal factor w evaluated at the vertex i , respectively. Given a Euclidean triangulation $T = (V, E, F)$ of (S, V) , associate each edge $ij \in E$ to two oriented half edges, one from i to j and the other from j to i . Let $E_{ij}(T)$ be the set of oriented edges in T starting at the vertex i and pointing to the vertex j . Note that $E_{ii}(T)$ may not be empty. Let $E_i(T)$ be the set of oriented edges in T starting from the vertex i , i.e., $E_i(T) = \cup_{j \sim i} E_{ij}(T)$. For an edge e shared by the triangles f and f' , let α_e and α'_e be the angles opposite e in f and f' , respectively. We have the following lemma on the curvature K .

Lemma 4.2.

- (i) K_i is a C^1 function on $\mathbb{R}^{|V|}$ for any vertex i .
- (ii) Let T be a Delaunay triangulation in the metric $w * d$; then

$$(4.3) \quad \frac{\partial K_i}{\partial w_j} = \begin{cases} -\sum_{e \in E_{ij}(T)} (\cot \alpha_e + \cot \alpha'_e) & \text{if } i \neq j, \\ \sum_{e \in E_i(T)} (\cot \alpha_e + \cot \alpha'_e) - \sum_{e \in E_{ii}(T)} (\cot \alpha_e + \cot \alpha'_e) & \text{if } i = j. \end{cases}$$

- (iii) The matrix $(\frac{\partial K_i}{\partial w_j})_{i,j}$ is semipositive definite, and its null space consists only of constant vectors.

Proof. For a $w \in \mathbb{R}^{|V|}$ such that $w * d$ is in the interior of a cell of $C(d)$, the above lemma was proved by Luo [29]. In fact, in our setting, because the triangulation T is Delaunay, we have $\alpha_e + \alpha'_e \leq \pi$ and thus $\cot \alpha_e + \cot \alpha'_e \geq 0$ for any edge e , which means the matrix $(\frac{\partial K_i}{\partial w_j})_{i,j}$ is diagonally dominant. So it remains to show that K_i is C^1 on the cell boundaries.

Assume T' is another Delaunay triangulation in the metric $w * d$. Since T and T' are related by a sequence of cocircular diagonal switches, we may assume T' is obtained from T by one cocircular diagonal switch. Assume the diagonal e of the quadrilateral $f \cup f'$ is switched to the other diagonal e' , as shown in the right picture of Figure 1. For any vertex i , K_i obviously remains the same before and after the diagonal switch. From (4.3), the evaluation of $\frac{\partial K_i}{\partial w_j}$ only involves the quantity $\cot \alpha_e + \cot \alpha'_e$ associated to any edge e . Observe that only for the sides and the diagonals of the quadrilateral $f \cup f'$ may this quantity differ before and after the diagonal switch. For the diagonal e , this quantity is 0 in T due to the fact that $\alpha_e + \alpha'_e = \pi$, and remains 0 in T' , as e is not an edge in T' , and similarly for another diagonal e' . For any side, say, e_1 (see Figure 1), as the angle opposite to e_1 in the triangle f equals the angle opposite to e_1 in the triangle f' , this quantity associated to e_1 remains the same before and after the diagonal switch. This shows that K_i is C^1 for any vertex i . ■

Define a differential one-form on the space of conformal factors as $\Omega(w) = \sum_{i=1}^n K_i(w) dw_i$ for any $w \in \mathbb{R}^n$. From (4.3), $\frac{\partial K_i}{\partial w_j} = \frac{\partial K_j}{\partial w_i}$ for any i, j , implying that Ω is closed and thus exact, as the domain \mathbb{R}^n is simply connected. This means the path integral of Ω depends only on the endpoints of the path. Given a prescribed curvature $K^* \in \mathbb{R}^n$, define the energy E over

the space of discrete conformal factors as

$$(4.4) \quad E(w) = \int_0^w \sum_{i=1}^n K_i(w) dw_i - \sum_{i=1}^n K_i^* w_i.$$

Note that the gradient of the energy $\nabla E = (K_1 - K_1^*, \dots, K_n - K_n^*)^t$ and the Hessian of the energy $H(E) = (\frac{\partial K_i}{\partial w_j})_{i,j}$. From Lemma 4.2, the Hessian $H(E)$ is semipositive definite, and thus the energy E is convex and strictly convex restricted to the subspace $W = \{w \in \mathbb{R}^n | w_1 + \dots + w_n = 0\}$. If the prescribed curvature K^* satisfies the conditions stated in Theorem 3.2, there exists a discrete conformal factor $w^* \in W$ such that $K^* = K(w^*)$. This means $\nabla E(w^*) = 0$, implying that w^* is the unique minimum of the energy E on the subspace W . Thus, one can employ Newton's method to find w^* and hence the PL metric $w^* * d$, which realizes the prescribed curvature.

5. Discrete conformal map. In this section, we construct a map $\phi : (S, V, d) \rightarrow (S, V, d')$ on the same marked surface (S, V) but with two PL metrics d and d' discrete conformal to each other, which we call the discrete conformal map from d to d' . In [14], given a PL metric d on (S, V) , we equip (S, V) with another hyperbolic metric with cusps (but no decorations) at V , denoted $h(d)$. We show that d' and d are discrete conformal to each other if and only if $h(d)$ and $h(d')$ are isometric to each other by an isometry homotopy to the identity. The discrete conformal map ϕ from d to d' is defined as that isometry from $h(d)$ to $h(d')$. In this paper, instead of establishing the connection to the hyperbolic metric, we give a more constructive description of the discrete conformal map for the purpose of better understanding the algorithm of explicitly constructing the map. To make it concrete, assume the triangulations $T = (V, E, F)$ and $T' = (V, E', F')$ are Delaunay under d and d' , respectively. Think of the surface (S, V, d) as the disjoint union of the Euclidean triangles in F with pairs of edges identified by isometries, and similarly for the surface (S, V, d') . Note that the map ϕ restricted to V is the identity map on V , and the task is to extend the map to the interiors of the edges in E and the interiors of the triangles in F .

Let $w \in \mathbb{R}^n$ be the conformal factor so that $d' = w * d$. First, we consider the special case where there is a triangulation T which is Delaunay in both d and d' ; i.e., d, d' are in the same cell $\mathcal{M}_D(T)$. In this case, the discrete conformal map is the so-called piecewise circumcircle preserving projective map introduced by Bobenko, Pinkall, and Springborn [4]. Let the triangles f_{ijk} and f'_{ijk} be the same triangle in T with the vertices i, j, k and the edge lengths measured in d and d' , respectively. Then the map $\phi|_{f_{ijk}} : f_{ijk} \rightarrow f'_{ijk}$ is defined in terms of the barycentric coordinates as

$$(5.1) \quad \phi|_{f_{ijk}}(u_i, u_j, u_k) = (u_i e^{-2w_i}/z, u_j e^{-2w_j}/z, u_k e^{-2w_k}/z),$$

where $z = u_i e^{-2w_i} + u_j e^{-2w_j} + u_k e^{-2w_k}$ is the normalizing factor. It is shown in [4] that the map $\phi|_{f_{ijk}}$ is a projective map from f_{ijk} onto f'_{ijk} which also maps the circumcircle of f_{ijk} to the circumcircle of f'_{ijk} . For two triangles f_{ijk} and f_{jil} sharing the edge e_{ij} , the maps $\phi|_{f_{ijk}}$ and $\phi|_{f_{jil}}$ coincide on the common edge e_{ij} . Thus, we can glue the maps on individual triangles together to form a globally continuous map, which by definition is the discrete conformal map $\phi : (S, V, d) \rightarrow (S, V, d')$. Note that the straight line remains straight within a triangle under the map ϕ as any projective map preserves straight lines.

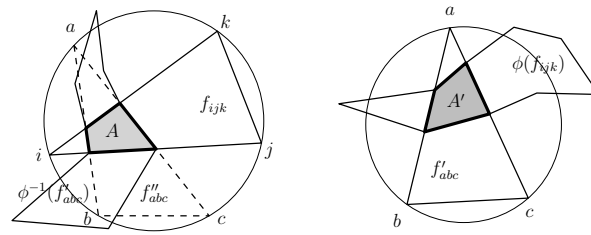


Figure 6. The mapping triangle of a polygonal facet of $T \cup T'$.

Next, we consider the general case where d and d' may not be in the same cell in $C(d)$. Consider a path $\gamma : [0, 1] \rightarrow C(d)$ with $\gamma(0) = d$ to $\gamma(1) = d'$. Let d_1, d_2, \dots, d_{m-1} be the intersections of γ with the boundaries of the cells in $C(d)$ listed in increasing order of their path parameter. See Figure 5 for an illustration. For convenience, let $d_0 = d$ and $d_m = d'$. For any $i = 0, 1, \dots, m - 1$, d_i and d_{i+1} are in the same cell $\mathcal{M}_D(T_i)$ for some triangulation T_i . Let $\phi_i : (S, V, d_i) \rightarrow (S, V, d_{i+1})$ be the discrete conformal map from d_i to d_{i+1} defined in the above special case. Then the discrete conformal map from d to d' by definition is the compositions of the above maps $\phi = \phi_0 \circ \phi_1 \circ \dots \circ \phi_m$.

We now state some properties of the discrete conformal map. For their proofs, interested readers are referred to the paper [14]. The most important property is that the map ϕ is independent of the choice of the path γ . Namely, if we choose another path γ' , we may end up with a different set of maps $\phi'_0, \phi'_1, \dots, \phi'_k$, but their composition gives the same map ϕ . Therefore, the map ϕ is indeed a well-defined map from d to d' . The second property is that a straight line on (S, V, d) remains straight within a triangle in T' under the map ϕ and similarly for a straight line on (S, V, d') under the inverse of ϕ . Another important property is that ϕ remains a piecewise circumcircle-preserving projective map but on the smaller pieces. Specifically, for two triangles $f_{ijk} \in T$ and $f'_{abc} \in T'$, let $A = f_{ijk} \cap \phi^{-1}(f'_{abc})$ and $A' = f'_{abc} \cap \phi(f_{ijk})$. If $A \neq \emptyset$, then $\phi(A) = A'$, and $\phi|_A : A \rightarrow A'$ is the restriction onto A of the circumcircle preserving projective map from a triangle f''_{abc} to the triangle f'_{abc} . The triangle f''_{abc} is constructed as follows. The preimage of the edges of f'_{abc} inside f_{ijk} are straight segments. See Figure 6 for an illustration. Extend them linearly to intersect the circumcircle of the triangle f_{ijk} . One can show that there are always exactly three intersection points. If we labeled the intersections according to the labels of the endpoints of the edges in f'_{abc} , this constructs the triangle f''_{abc} , which we call the *mapping triangle* of A . Let $d'(st)$ and $d''(st)$ be the lengths of the edge st in f'_{abc} and f''_{abc} , respectively, for any $\{s, t\} \subset \{a, b, c\}$. Calculate $w'_a = \left(\frac{d'(ab)d'(ac)}{d'(bc)}\right)^{1/2}$ and similarly for w'_b, w'_c . Then by replacing w by w' in (5.1), we construct the circumcircle-preserving projective map from f''_{abc} to f'_{abc} .

For the surface (S, V) with boundary, one can verify that the straight line which cuts the region $\cup_{f \in F_s(T_i)} f$ into two identical subregions (see Figure 4) is the image of the segment s under the discrete conformal map $\tilde{\phi}$. Therefore, if we let $\tilde{\phi}$ denote the discrete conformal map on the doubled surface, then the restriction of $\tilde{\phi}$ onto a copy of S is a map from (S, V, d) to (S, V, d') , which we define as the discrete conformal map ϕ from (S, V, d) to (S, V, d') .

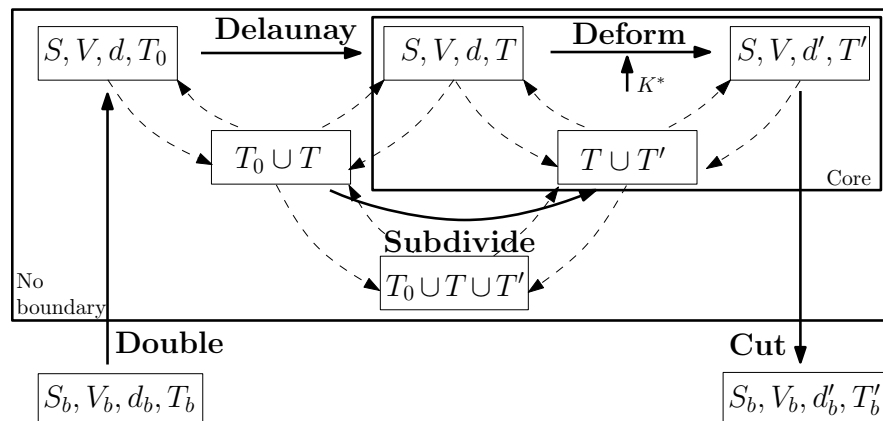


Figure 7. The main objects and the procedures of the algorithm for solving the problem of prescribing curvature.

6. Algorithm. We have presented the main ideas of the algorithm for solving the problem of prescribing curvature. In this section, we give more details of the algorithm at the implementation level.

The main objects and the procedures used in the algorithm are shown in Figure 7. In the problem of prescribing curvature, assume we are given a closed surface S with a Euclidean triangulation $T = (V, E, F)$ which is Delaunay, and a desired curvature $K^* : V \rightarrow \mathbb{R}$. Note that the initial PL metric d on (S, V) is determined by the edge lengths of the Euclidean triangles in T . The goal of the algorithm is (1) to find a triangulation $T' = (V, E', F')$ on S and an edge length assignment l' over the edges in E' so that the PL metric d' on (S, V) determined by l' is discrete conformal to d and the curvature of d' equals K^* , and (2) to construct the discrete conformal map ϕ from d to d' . This is the core of the algorithm, which is performed by the procedure “Deform” using Newton’s method described in section 4. In many applications, the given Euclidean triangulation T_0 on S may not be Delaunay. The procedure “Delaunay” is employed to convert T_0 to a Delaunay triangulation T under the same PL metric by diagonal switches, as described in [10]. Moreover, if the initial surface has boundaries, the procedure “Double” is to double the surface to remove the boundary, and the procedure “Cut” is to cut out a copy of the deformed surface from the deformed doubled surface, as described in section 3.1. Both the procedures “Double” and “Cut” are straightforward to implement.

The procedure “Deform” deforms the metric and also changes the triangulations, as shown in Algorithm 1, whose implementation is more involved than the other procedures. Note that the discrete conformal map ϕ is a piecewise circumcircle preserving projective map on the pieces of the common refinement of the triangulations T and T' , denoted $T \cup T'$. Topologically, the refinement $T \cup T'$ is also a polyhedral surface whose vertices consist of the vertices V and the intersections of the edges in T with the edges in T' . To see the geometry of $T \cup T'$, consider the discrete conformal map $\phi : (S, V, d) \rightarrow (S, V, d')$. According to the theory of discrete conformal mapping described in [14], an edge in T' is pulled back to (S, V, d) and geometrically becomes a polygonal line which is straight inside a triangle of T . Similarly, an

Algorithm 1. Deform($T = (V, E, F)$, l_T , K^* and ϵ).

- 1: Initialize $T \cup T' = T' = T$
- 2: Set $w = 0$;
- 3: Evaluate $K(w)$ and set $\nabla E = K(w) - K^*$
- 4: **while** $\|\nabla E\| > \epsilon$ **do**
- 5: Evaluate $H(E)$ and set $\Delta w = H(E)^{-1} \nabla E$
- 6: MoveTo(w , $w - \Delta w$, T' , $T \cup T'$, $l_{T'}$)
- 7: $w \leftarrow w - \Delta w$
- 8: **end while**
- 9: Output T' , $T \cup T'$, $l_{T'}$.

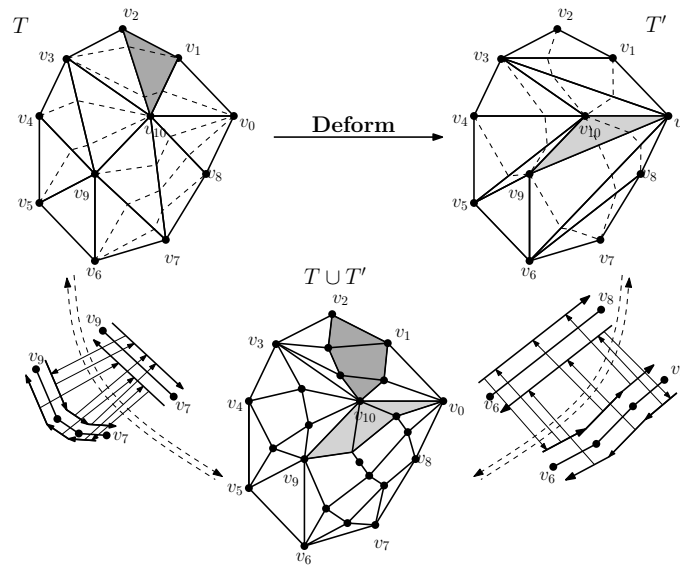


Figure 8. Refinement: The dotted lines in T are the images of the edges in T' under the discrete conformal map from d to d' , which are straight within a triangle in T , and similarly for the dotted lines in T' .

edge in T is pushed forward to (S, V, d') and is straight within a triangle of T' . Therefore, each edge of $T \cup T'$ is geometrically straight on both (S, V, d) and (S, V, d') . See Figure 8 for an illustration. For instance, the triangle $v_1 v_2 v_{10}$ in T is subdivided into three polygonal facets in $T \cup T'$ and similarly for the triangle $v_9 v_0 v_{10}$ in T' . All of the involved polyhedral surfaces are represented by halfedge data structures. A mechanism is built for these polyhedral surfaces to communicate with each other as follows: each edge in T or T' has access to its first subedge in $T \cup T'$, and each edge in $T \cup T'$ has access to the edge in T and/or T' to which it belongs. In the example shown in Figure 8, for instance, each halfedge of the edge $v_7 v_9$ in T has a pointer pointing to its first subhalfedge in $T \cup T'$ and similarly for the halfedges of $v_6 v_8$ in T' . At the same time, each subhalfedge of $v_7 v_9$ ($v_6 v_8$) in $T \cup T'$ is equipped with a pointer pointing back to the corresponding halfedge of $v_7 v_9$ in T ($v_6 v_8$ in T').

The final PL metric is determined by the edge length assignment $w *_{T'} l_{T'}$ over the edges in T' . For a vertex v of $T \cup T'$ which is the intersection of an edge e in T and an edge e' in T' in

Algorithm 2. MoveTo($w_1, w_2, T', T \cup T', l_{T'}$).

- 1: Assume $w(t)$ with $t \in [0, 1]$ is a path satisfying $e^{-2w(t)} = (1-t)e^{-2w_1} + te^{-2w_2}$.
 - 2: Let the edge e in T' be the first edge that fails the Delaunay condition along the path $w(t)$.
 - 3: **if** e exists **then**
 - 4: Assume e fails to be Delaunay at $w(t_1)$.
 - 5: Switch the edge e , and update $l_{T'}$.
 - 6: Update $T \cup T'$: (i) for the newly generated polygons, compute the edge lengths of their mapping triangles, and (ii) for the vertices of $T \cup T'$ which are not the vertices of T' , compute their new positions on the edges of T' under the edge length assignment $w(t_1) *_{T'} l_{T'}$.
 - 7: MoveTo($w(t_1), w_2, T', T \cup T', l_{T'}$).
 - 8: **else**
 - 9: For the vertices of $T \cup T'$ which are not the vertices of T' , compute their new positions on the edges in T' with the edge length assignment $w_2 *_{T'} l_{T'}$.
 - 10: **end if**
 - 11: Output $T', T \cup T', l_{T'}$, and w .
-

the interior, we store both of its positions on e and e' . In this way, we can visualize $\phi^{-1}(e)$ for any edge e in T' on the input surface (S, V, d) , and $\phi(e)$ for any edge e in T on the deformed surface (S, V, d') . For a polygon A in $T \cup T'$, we store the edge lengths of its mapping triangle for the purpose of constructing the discrete conformal map ϕ . In each iteration in Newton's method, the conformal factor w is updated to $w - \Delta w$, which may change the triangulation T' , the refinement $T \cup T'$, and $l_{T'}$ as well. The subprocedure "MoveTo" shown in Algorithm 2 presents more details on how to update the conformal factor and the combinatorial structures of T' and $T \cup T'$.

Let $l_e = l_{T'}(e)$ for an edge e in T' and $x(u) = e^{-2w(u)}$. Consider an edge e as shown in Figure 1. That e is Delaunay is by cosine law equivalent to

$$(6.1) \quad \frac{l_{e_1}l_{e'_1} + l_{e_2}l_{e'_2}}{l_{e_1}l_{e'_2}}x(v) + \frac{l_{e_1}l_{e'_1} + l_{e_2}l_{e'_2}}{l_{e_2}l_{e'_1}}x(u) - \frac{l_e^2}{l_{e_1}l_{e_2}}x(u') - \frac{l_e^2}{l_{e'_1}l_{e'_2}}x(v') \geq 0,$$

which is a linear constraint in the variables x . Thus if we change the variables from w to x , the cell $C(d) \cap \mathcal{M}_D(T')$ becomes a convex polytope. We choose a path from w to $w + \Delta w$ so that it is a line segment in the variables x . This makes it easy to detect which edge to switch first as it amounts to computing the intersections of the line segment with the hyperplanes defined by the linear constraints.

Finally, the purpose of constructing the refinements $T_0 \cup T$ and $T_0 \cup T \cup T'$ is for visualization. When the input Euclidean triangulation T_0 on S is embedded in \mathbb{R}^3 , we can pull back the triangulations T and T' onto T_0 for the purpose of visualization. The common refinement of the triangulations T_0 and T , denoted $T_0 \cup T$, is also computed in the procedure "Delaunay." The procedure "Subdivide" computes the common refinement of the triangulations of T_0, T , and T' . In this way, we can pull back the edges in T back to T_0 under the identity map over (S, V, d) , and the edges in T' back to T_0 under the discrete conformal map ϕ from d to d' .

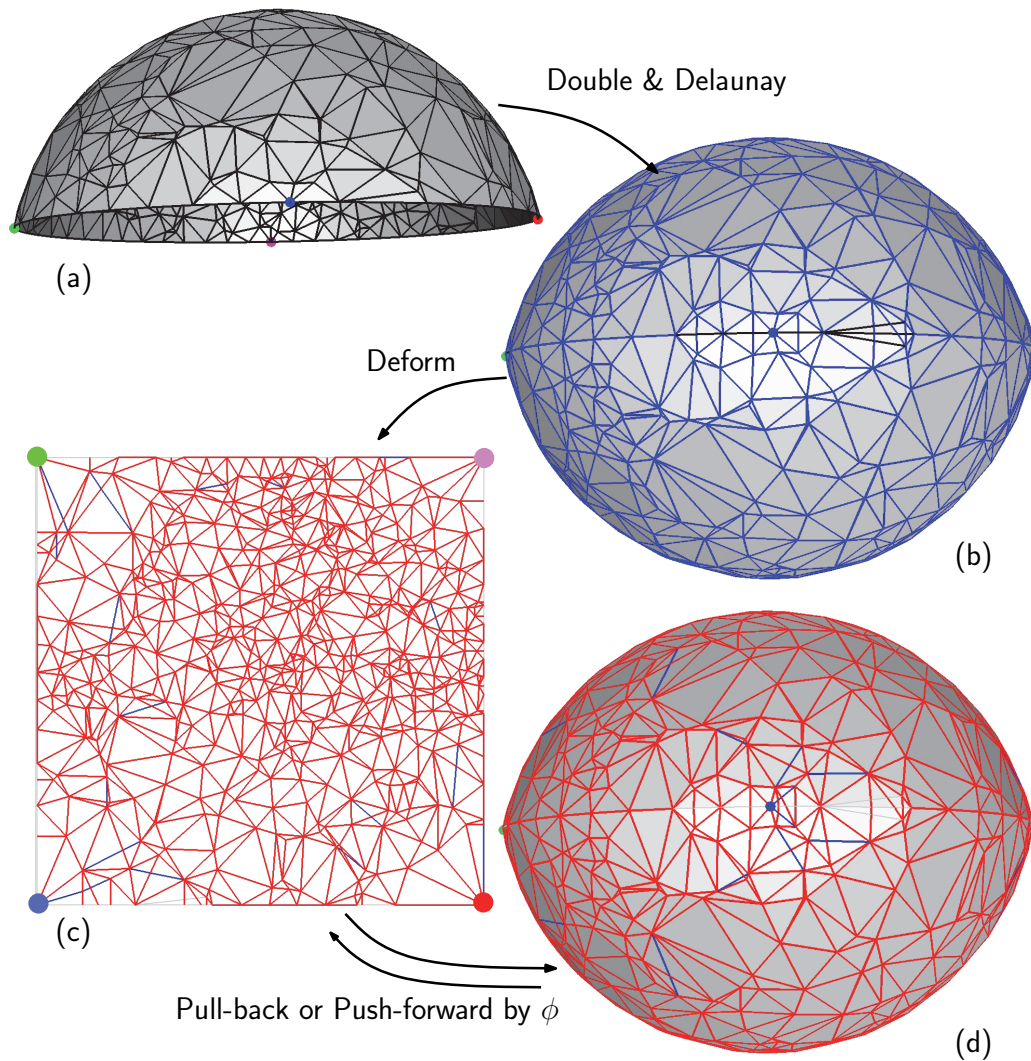


Figure 9. (a) The polyhedral surface (S_b, V_b, d_b, T_b) of a spherical cap. (b) The doubled polyhedral surface. The Delaunay triangulation T consists of the triangles with blue edges. The black edges are non-Delaunay edges in the triangulation T_0 . (c) Half of the doubled polyhedral surface after discrete conformal deformation. The Delaunay triangulation T' consists of the triangles with red edges. The blue edges are the push-forward of the switched edges in T under the discrete conformal map ϕ . Note that the blue edges may not be straight. (d) The triangles with red edges are the pull-back of the edges in T' under the map ϕ . Note that the red edges may not be straight.

Figure 9 shows the results of the different procedures when the algorithm runs over the polyhedral surface of a spherical cap. In this example, we can embed the doubled polyhedral surface into \mathbb{R}^3 and visualize both the triangulations T_0 and T (Figure 9(b)). Moreover, we can visualize the pull-back of the triangulation T' under the map ϕ (Figure 9(d)). In addition, we set the target curvature 0 everywhere except at four marked points on the boundary where it is set to be $\pi/2$. In this way, we can embed the deformed polyhedral surface into a rectangle,

as shown in Figure 9(c). We use the procedure described in [17] to lay out a flat surface into the plane. Note that in all the examples shown in the paper, we fix the ϵ in Algorithm 1 to be 10^{-5} .

7. Experimental results. In this section, we will show numerical examples, demonstrate numerically the convergence of our discrete conformality, and compare this to the state of the art. For convenience, we follow the notation in Figure 7 and denote T_0 the (doubled) input triangulation, and T and T' the Delaunay triangulations under the initial metric d and the deformed metric d' , respectively.

7.1. Simple examples. In this subsection, we show a few examples with a small number of triangles for a clear illustration of the geometric deformation of the metric and the combinatorial changes of the triangulation. In the first couple of examples, to visualize the resulting metric, we prescribe the curvature to be zero except at a few vertices in order to satisfy the Gauss–Bonnet theorem. A vertex with nonzero curvature is called *singular*. The first example is a polyhedral surface of topological sphere, which we call *Star*, shown in the left column of Figure 10. The total curvature of *Star* is 4π . We choose three singular vertices as marked in Figure 10(a), where the curvature is set to be $\frac{4\pi}{3}$. To embed the deformed *Star* into the plane, we cut *Star* along a tree of the edges in T' passing through three singular vertices. The tree is shown in green in Figure 10(a). The planar embedding of the deformed *Star* is shown in Figure 10(b), where the red edges are the edges of the triangulation T' and the blue edges are the images of the switched edges in the triangulation T under the discrete conformal map ϕ . The red edges in Figure 10(c) are the preimage of the edges in the triangulation T' under the map ϕ . The second example is a polyhedral surface of genus two which we call *Eight*, shown in the right column of Figure 10. The total curvature of *Eight* is -4π . We choose one singular vertex as marked in Figure 10(b), whose curvature is set to be -4π . To embed the deformed *Eight* into the plane, we cut *Eight* along a cut graph consisting of the edges in T' passing through the singular vertex. The cut graph is shown in green in Figure 10(d). The planar embedding of the deformed *Eight* is shown in Figure 10(e). The red and blue edges in Figure 10(e,b) have the same meaning as those in *Star*. The gray edges are the non-Delaunay edges in the triangulation T_0 .

The main purpose of the next couple of examples is to show the triangulation of T' when we prescribe a curvature close to the boundary of the domain of all possible curvatures. In both examples, the curvature is prescribed to be $2\pi - 0.1$ at every vertex except at one vertex (labeled a for later reference), whose curvature is set to satisfy the Gauss–Bonnet theorem and is usually a negative value. In the example of *Star*, the prescribed curvature at the vertex a is $-22\pi + 1.4$, and in the example of *Eight*, it is $-58\pi + 2.7$. In Figure 11, the red edges are the preimage of the edges in the triangulation T' pulled back by the discrete conformal map ϕ into the input surface. Every triangle in T' has a as its vertex. In fact, in these two examples, at least two of three vertices of any triangle in T' are a .

7.2. Convergence. In this subsection, we will present numerical evidences showing the convergence of our discrete conformality. In addition, we will demonstrate the efficiency and the robustness of our algorithm, in particular against the quality of the input triangulations, and compare its performance to the state of the art. We check how much the conformality is

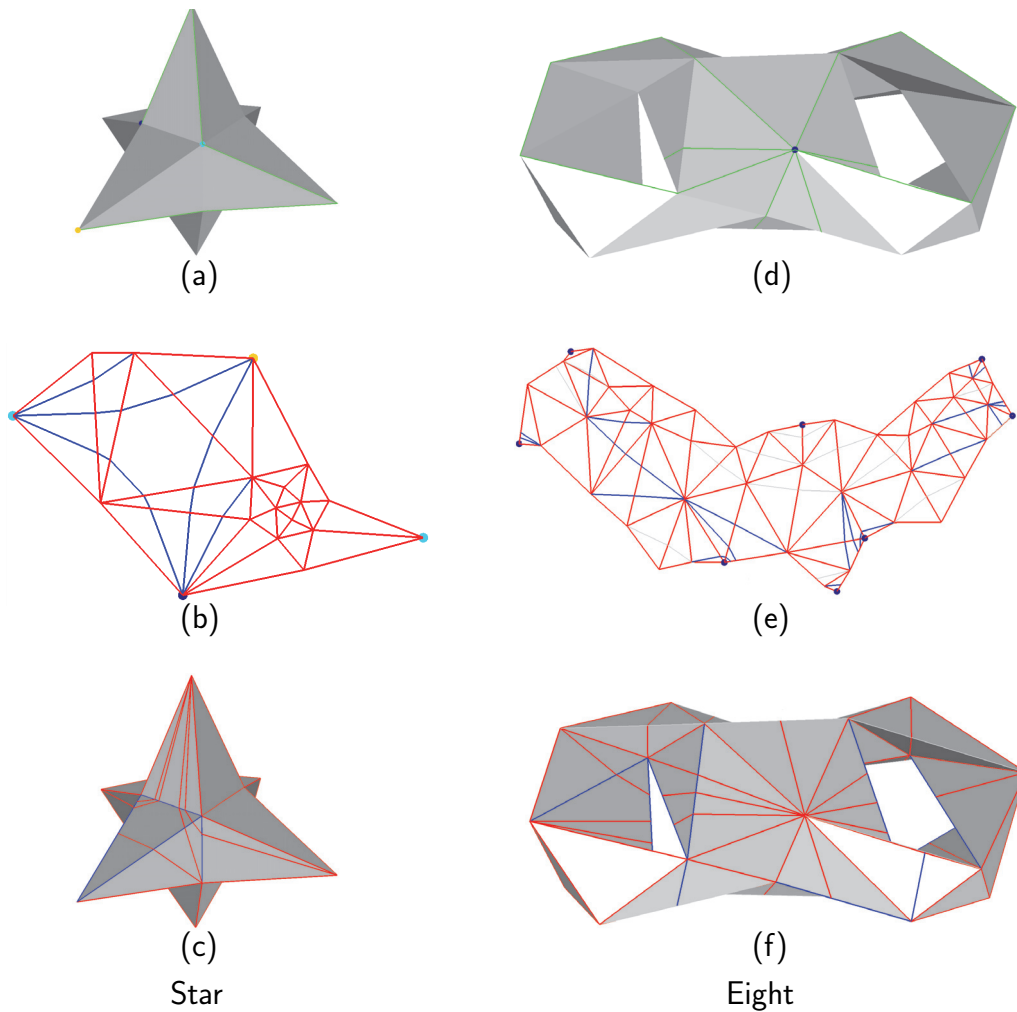


Figure 10. (a), (d) The original polyhedral surfaces. The marked vertices have nonzero prescribed curvature. The green edges show a tree (a cut graph) passing the marked vertices. (b), (e) The planar embedding of the deformed polyhedral surfaces after cutting them open along the tree (the cut graph). The red edges are the edges in the triangulation T' , and the blue edges are the images of the switched edges in the triangulation T under the discrete conformal map ϕ . (c), (f) The red edges are the preimages of the edges in the triangulation T' under the map ϕ , and the blue edges are the edges in T that were switched during the conformal deformation. The gray edges in (b), (c), (e), and (f) are the non-Delaunay edges in the triangulation T_0 .

preserved when the triangulated surfaces are flattened into the plane, and we use two types of criteria to measure the conformality.

7.2.1. Criteria. For the examples where the (approximated) ground truth of conformal flattening is known, we can compare the results with the ground truth. Let u_{gt} be the flattening map of the (approximated) ground truth, and let u be the flattening map constructed by our algorithm or other methods described below. We use the following two norms to measure the

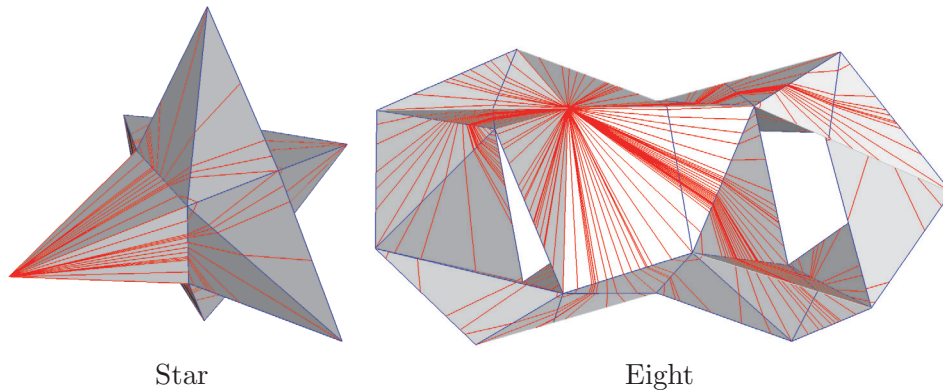


Figure 11. The color scheme of the edges is the same as that in Figure 10(c, f).

approximation error:

$$(7.1) \quad e_2 = \left(\frac{\sum_{i \in V} \|u(i) - u_{gt}(i)\|^2 A_i}{\sum_{i \in V} A_i} \right)^{1/2} \quad \text{and} \quad e_\infty = \max_{i \in V} \{\|u(i) - u_{gt}(i)\|\}.$$

where A_i is the area weight, which is estimated as a third of the total area of the triangles in T incident to the vertex i .

In general, the ground truth of conformal flattening is not known. Given an orientation preserving map h between two Riemann surfaces, the Beltrami coefficient is $\mu = \frac{h_z}{h_{\bar{z}}}$, where z is a complex number representing the local coordinates. The map h sends an infinitesimal circle to an infinitesimal ellipse with the ratio of major semiaxis to minor semiaxis equal to $D(h) = \frac{1+|\mu|}{1-|\mu|}$. Note that $|\mu| < 1$ as the map h preserves orientation. $D(h)$ is called the conformal distortion of the map h and $D(h) = 1$ if and only if h is conformal. So we check the conformality of the map h by measuring how far $D(h)$ is away from 1. Specifically, we estimate $\|D(h) - 1\|_{L_2}$ and $\|D(h) - 1\|_{L_\infty}$.

Let $(S, T = (V, E, F))$ be the input triangulated surface. In the methods we describe below for comparison, the constructed flattening map h is piecewise linear; namely, on a triangle $f \in F$, $h|_f$ is the linear extension of the map on the vertices of the triangle. Let $L_f(z) = \alpha z + \beta \bar{z}$ represent the linear map $h|_f$. The conformal distortion of this linear map L_f can be computed as $D(L_f) = \frac{|\alpha+|\beta|}{|\alpha-|\beta|}$. For a piecewise linear flattening map h , we have

$$(7.2) \quad \|D(h) - 1\|_{L_2} = d_2 = \left(\frac{\sum_{f \in F} (D(L_f) - 1)^2 \text{area}(f)}{\sum_{f \in F} \text{area}(f)} \right)^{1/2} \quad \text{and}$$

$$(7.3) \quad \|D(h) - 1\|_{L_\infty} = d_\infty = \max_{f \in F} \{D(L_f) - 1\}.$$

In our method, from the discussion in section 5, the constructed flattening map h is piecewise circumcircle-preserving projective. Specifically, for a polygonal face A in the common refinement $T \cup T'$, let f and f' be the triangle in T and T' containing A . The map h restricted to A , denoted $h|_A$, is the restriction to A of the circumcircle preserving projective map from the

mapping triangle f'' to the triangle f' . Let $L_A(z) = \alpha z + \beta \bar{z}$ be the linear map from f'' to f' . In [14], we have shown that $D(h|_A) \leq D(L_A)$. Therefore, for our flattening map h , we have the following upper bounds on $\|D(h) - 1\|_{L_2}$ and $\|D(h) - 1\|_{L_\infty}$, which are easy to estimate:

$$(7.4) \quad \|D(h) - 1\|_{L_2} \leq d_2 = \left(\frac{\sum_{A \in F(T \cup T')} (D(L_A) - 1)^2 \text{area}(A)}{\sum_{f \in F(T \cup T')} \text{area}(A)} \right)^{1/2} \quad \text{and}$$

$$(7.5) \quad \|D(h) - 1\|_{L_\infty} \leq d_\infty = \max_{f \in F} \{D(L_A) - 1\},$$

where $F(T \cup T')$ denotes the set of the polygonal faces in $T \cup T'$ and $\text{area}(A)$ denotes the area of A as a subset of the triangle f .

7.2.2. Conformal flattening methods. We briefly describe three methods, including ours, of conformally flattening triangulated surfaces into the plane.

Method of discrete conformal deformation (DC). This flattening method is based on our discrete conformal deformation. To flatten a triangulated surface into the plane, we basically prescribe the curvature to be 0 and solve the problem of prescribing curvature using the algorithm described in section 6. Due to the obstruction of topology, the target curvature cannot be 0 everywhere. We call those whose curvature are not zero the singular vertices. For a topological disk surface, we choose three singular vertices on the boundary and set the curvature there to be $2\pi/3$. In this way, we flatten a triangulated surface of a topological disk onto an equilateral triangle. This flattening map is guaranteed to be one to one. For a topological sphere surface, as we did in section 7.1 for Star, we choose three singular vertices whose curvatures are set to be $4\pi/3$, and we cut the surface along a tree of the edges in T' passing through the singular vertices for flattening the triangulated surface. For a surface of genus $g \geq 1$, we choose $2(g-1)$ singular vertices whose curvatures are set to be -2π , and we cut the surface along a cut graph consisting of the edges in T' and passing the singular vertices for flattening the triangulated surface.

Method of holomorphic form (HF). Gu and Yau [16] proposed a method to conformally flatten a surface of genus $g \geq 1$ into the plane using holomorphic one-forms. Assume $h = f(z)dz$ is a holomorphic one-form of the surface; it is well known that the metric $|f(z)|^2 dz d\bar{z}$ is conformal and flat when $f(z) \neq 0$. Noticing that any holomorphic one-form can be decomposed as $h = \omega + i(*\omega)$, where ω is a real harmonic one-form and $*\omega$ is its conjugate, Gu and Yau developed discrete algorithms for approximating from a triangulated surface a basis $\{\omega_1, \dots, \omega_{2g}\}$ of the space of real harmonic one-forms and their conjugates $*\omega_1, \dots, *\omega_{2g}$. Then $\{h_1 = \omega_1 + i(*\omega_1), \dots, h_{2g} = \omega_{2g} + i(*\omega_{2g})\}$ contains a basis of the space of holomorphic one-forms, and any linear combination $h = \sum_i a_i h_i$ is a holomorphic one-form. Integrate the real part and the imaginary part of h along the edges of the triangulated surface to obtain the x -coordinates and the y -coordinates, respectively, for the vertices. Note that the x, y -coordinate functions computed by integration are multivalued at a subset of vertices. The edges with both endpoints multivalued form a cut-graph of the surface. Cut the surface along this cut-graph and obtain a fundamental domain of the surface. The x, y -coordinate functions conformally map this fundamental domain into a planar region. For surfaces with boundary, one can double the surface to remove the boundary by gluing two copies along the boundary,

apply the above algorithm, and take half of the computed planar embedding. For a surface with topological disk, in order to obtain an embedding onto unit disk, the following procedure is used: (1) remove a triangle from the given triangulated surface to make an annulus; (2) apply the above algorithm to obtain an planar embedding of rectangular shape; (3) take the exponential to map the rectangle domain into an annulus with unit outer radius, and put back the removed triangle to obtain the final embedding onto the unit disk. In our experiments, we use the implementation made available to us by the authors.

Method of bounded distortion (BD). Lipman [27] considered the problem of finding a piecewise linear map h mapping a triangulated surface into the plane so that the conformal distortion $D(h)$ is less than some prescribed number C . This amounts to solving a nonconvex optimization problem, which was reduced to a conic optimization problem by restricting the domain of optimization to a convex subset. In [27], Lipman also proposed a binary search strategy to find a map with the “optimal” conformal distortion. Note that the reduced conic optimization may miss a map with the conformal distortion less than the prescribed number, and thus gives a wrong feedback to the binary search, which therefore may not reach a map with true optimal conformal distortion. In our experiments, the following iterative procedure is used to find a map with small conformal distortion, which is more efficient compared to the binary search strategy. In each iteration, assume a piecewise linear map h^k is given, construct a convex set of maps whose conformal distortion is less than $\|D(h^k)\|_\infty$, and then use the conic optimization to find the next map h^{k+1} in this convex set. The iteration is started with the Tutte embedding where the position of an interior vertex is the average of the positions of its neighboring vertices, and iterated at most 10 times. For vertices on the boundary, we fix the positions of three of them and impose the linear constraints on the others so that the resulting range is a triangle. The optimization package MOSEK [3] is used for conic optimization. In our experiments, we use the implementation made available to us by the author.

7.2.3. Examples. Now we run the above conformal flattening methods over several examples to show their performance, in particular to compare their convergence properties.

Spherical Cap. A spherical cap is a portion of a sphere cut off by a plane, which can be conformally flattened onto a unit disk by composing the stereographic projection with a scaling. So in this example, we have the ground truth for conformal flattening, denoted as u_{gt} . We run the aforementioned methods over four continuously refined triangulated surfaces with approximately 1000, 4000, 16000, and 64000 vertices, which are obtained by applying Cocone [2], a surface reconstruction algorithm, to the randomly drawn samples on the spherical cap and some additional samples on its boundary. Figure 12 shows the triangulated surfaces with 1000 and 4000 vertices.

For the methods of DC and BD, we choose three vertices $\{a, b, c\}$ on the boundary so that they are mapped to the vertices of an equilateral triangle. To compare with the ground truth, we use the Schwarz–Christoffel mapping, which can explicitly evaluate the conformal transformation mapping the unit disk onto a triangle. In fact, we use the Schwarz–Christoffel Toolbox [9] to compute the inverse map sending a, b, c to $u_{gt}(a), u_{gt}(b), u_{gt}(c)$, respectively. In the method of HF, we have already embedded the spherical cap onto the unit disk. We align the computed embedding to the ground truth by a Möbius transformation.

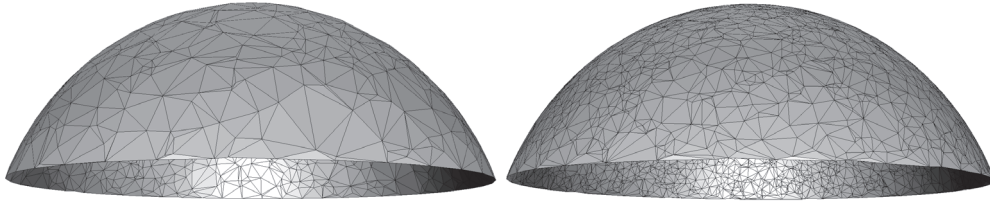


Figure 12. The triangulated surfaces of Spherical Cap with 1000 (left) and 4000 (right) vertices.

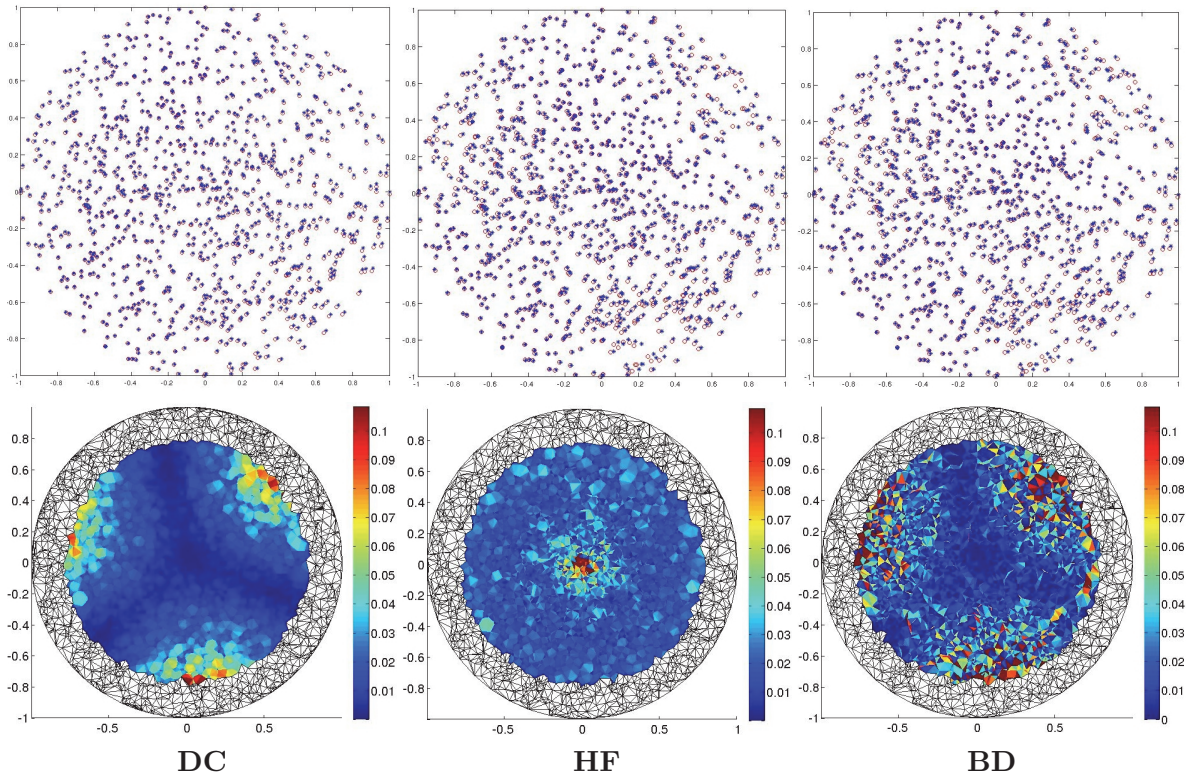


Figure 13. Results for Spherical Cap: The first row shows the planar embedding of the vertices for the triangulated surface with 1000 vertices. Blue *'s denote the ground truth, and the red \circ 's denote the results computed by different methods. The second row plots the conformal distortion $D(h) - 1$ of the planar embedding computed by different methods from the triangulated surface with 4000 vertices. Note that for the purpose of comparison, the range of the color map is fixed at $[0, 0.11]$, although the maximal conformal distortion of the planar embedding by HF and BD is larger than 1.11, as shown in Table 1.

The first row of Figure 13 shows the embedding of the vertices computed by different methods. In Table 1, we show the approximation errors, e_2 , e_∞ , d_2 , d_∞ , and the timing in seconds used by different conformal flattening methods to compute the embedding. Note that since the convergence is often stated for a compact region away from the boundary, we estimate the errors e_2 and e_∞ over the vertices which are mapped onto the disk D of radius 0.8, and the errors d_2 and d_∞ over the polygons or triangles whose vertices are mapped onto the disk D . In the second row of Figure 13, we only plot the conformal distortion of those

Table 1

Spherical Cap: Approximation errors and running time.

Method	1000	4000	16000	64000
DC	(0.0102, 0.0137)	(0.0034, 0.0048)	(0.0014, 0.0020)	(0.0010, 0.0014)
HF	(0.0023, 0.0078)	(0.0010, 0.0036)	(0.0011, 0.0030)	(0.0009, 0.0016)
BD	(0.0131, 0.0300)	(0.0054, 0.0150)	(0.0040, 0.0092)	(0.0023, 0.0051)
(e_2, e_∞)				
DC	(0.0505, 0.1592)	(0.0303, 0.1084)	(0.0160, 0.0570)	(0.0082, 0.0377)
HF	(0.0638, 12.9485)	(0.0270, 1.4460)	(0.0169, 1.3563)	(0.0085, 0.8276)
BD	(0.0829, 0.6582)	(0.0547, 0.9318)	(0.0313, 1.0055)	(0.0192, 1.1988)
(d_2, d_∞)				
DC	0.152	0.636	4.54	26.9
HF	1.03	3.14	12.7	53.7
BD	28.4	182	744	3395
timing (sec)				

polygons or triangles used to evaluate d_2 and d_∞ .

From Table 1, three methods all converge about linearly in terms of the e_2 , e_∞ , and d_2 errors. In terms of the absolute value of these approximation errors, BD performs worse than DC and HF. Only DC has a convergent d_∞ error, which is approximately linear. In terms of running time, DC and HF have a similar performance, while BD is much slower.

Hexagonal Mesh. The Riemann mapping from a planar region to unit disk can be approximated using Thurston's circle packing. Consider a hexagonal triangulation inside a planar region. One can explicitly construct a circle packing of unit disk, which is a collection of closed disks inside a unit disk having the following properties: (1) the interiors of the disks are disjoint; (2) the nerve of this collection of disks is isomorphic as a graph to the 1-skeleton of the hexagonal triangulation; (3) the boundary of the disk corresponding to each boundary vertex of the hexagonal triangulation tangentially touches the unit circle. This construction induces a map, denoted u_{gt} , from the hexagonal triangulation into the unit disk by mapping the vertices of the hexagonal triangulation to the centers of the corresponding disks and extending linearly to the triangles. Figure 14 shows two hexagonal triangulations inside a fixed planar region and their corresponding circle packings of the unit disk. Rodin and Sullivan [34] showed that the above-induced map converges to the Riemann mapping from the planar region to the unit disk as the size of the triangles in the hexagonal triangulation goes to 0.

We run the aforementioned methods over four continuously refined hexagonal triangulations of a planar region of the side lengths 0.2, 0.1, 0.05, and 0.025. The number of vertices in those triangulations is approximately 1000, 4000, 16000, and 64000. The first row in Figure 14 shows the input hexagonal triangulations. Note that a circle packing in the unit disk of a triangulation is not unique. We normalize the circle packing by choosing a vertex, denoted o for later reference, from the hexagonal triangulation and mapping it to the origin. The remaining freedom is a rotation, which, however, does not affect the consistency of the error estimations. To make the normalization consistent across different hexagonal triangulations, the four chosen vertices o (one from each triangulation) have the same coordinate. See the second row in Figure 14 for the resulting circle packings of the hexagonal triangulations.

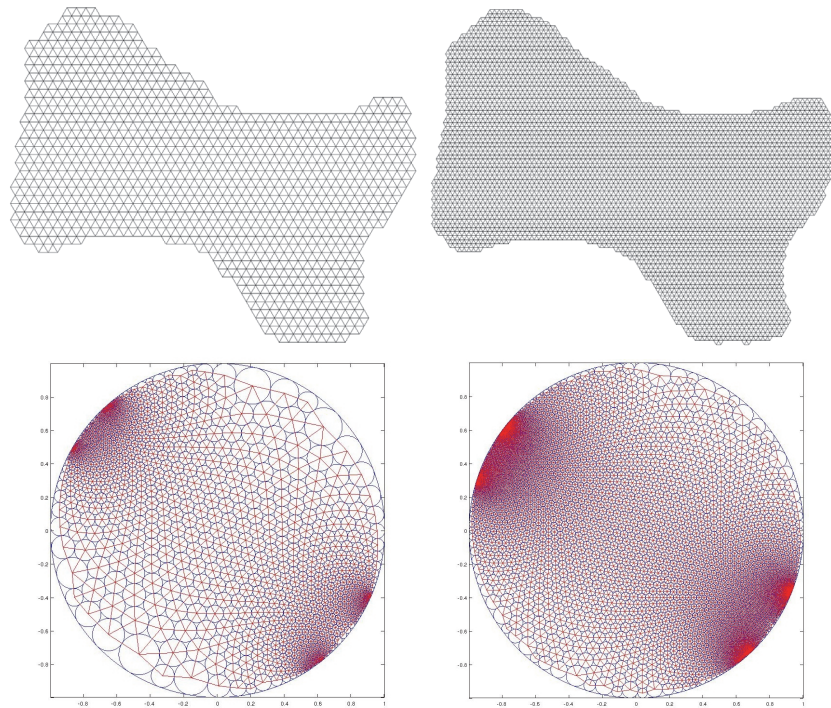


Figure 14. Hexagonal meshes and their circle packing. First row: The input hexagonal triangulations with 1000 vertices (left) and 4000 vertices (right). Second row: The circle packing in unit disk to the hexagonal triangulation above.

For the DC and BD methods, we again choose three vertices $\{a, b, c\}$ on the boundary so that they are mapped to the vertices of an equilateral triangle, and then we map the equilateral triangle onto the unit disk by the inverse of the Schwarz–Christoffel mapping, and finally we employ an automorphism of the unit disk to obtain the map u with $u(o) = 0$ and $\arg(u(a)) = \arg(u_{gt}(a))$. For the HF method, we also apply an automorphism of the unit disk to the computed embedding to obtain the same alignment.

Similarly, since the convergence is often stated for a compact region away from the boundary, we estimate the errors e_2 and e_∞ over the vertices which are more than 0.4 away from the boundary of the planar region, and the errors d_2 and d_∞ over the polygons or triangles with their vertices satisfying the same requirement. The first row of Figure 15 shows the embedding of the vertices computed by different methods, and the second row of Figure 15 plots the conformal distortion of the approximated Riemann mapping by different methods. In Table 2, we show the approximation errors e_2 , e_∞ , d_2 , d_∞ and the timing in seconds used by different conformal flattening methods for computing the embedding. In Table 2, a similar pattern as Spherical Cap is observed: all of the methods show linear convergence in the errors e_2 , e_∞ , d_2 , and DC remains converging linearly in the d_∞ error. In this example, BD becomes linearly convergent in the d_∞ error. This may be due to the fact that the triangles are all well shaped in the hexagonal triangulations.

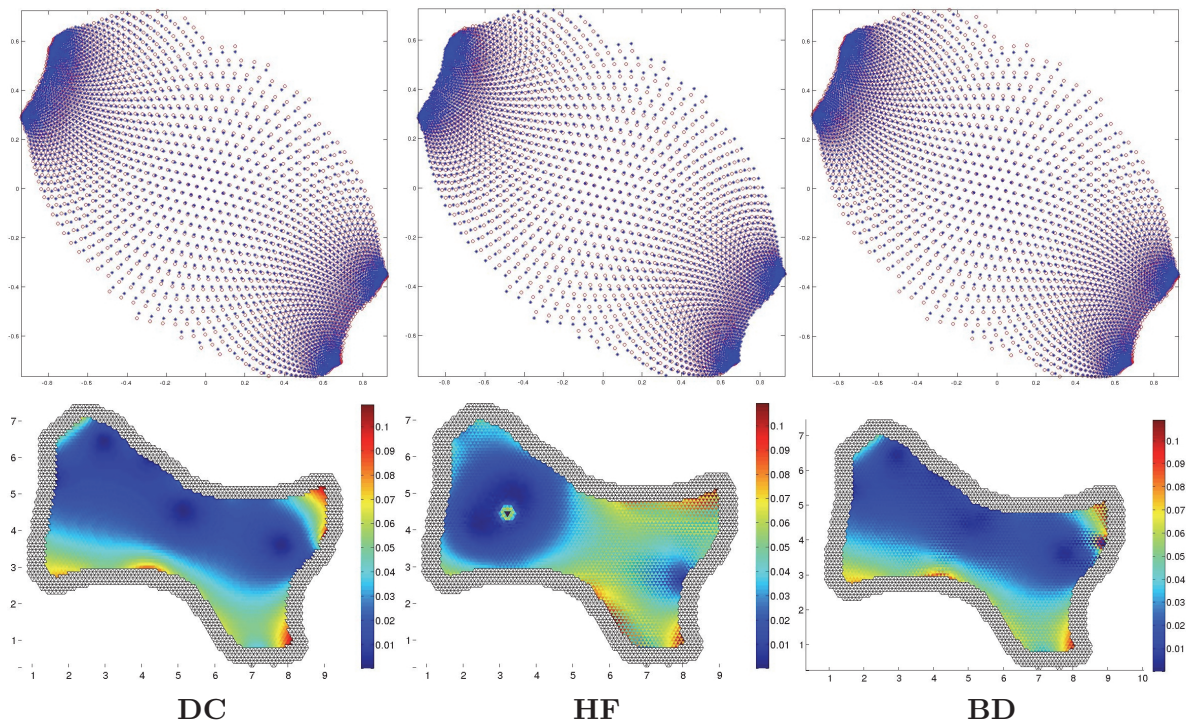


Figure 15. Results for Hexagonal Mesh: The first row shows the planar embedding of the vertices for the triangulated surface with 1000 vertices. Blue *'s denote the ground truth, and the red \circ 's denote the results computed by different methods. The second row plots the conformal distortion $D(h) - 1$ of the planar embedding computed by different methods from the triangulated surface with 4000 vertices. Note that for purposes of comparison, the range of the color map is fixed at $[0, 0.11]$, although the maximal conformal distortion of the planar embedding by HF and BD is larger than 1.11.

Table 2

Hexagonal Mesh: Approximation errors and running time.

Method	1000	4000	16000	64000
DC	(0.0257, 0.0486)	(0.0133, 0.0266)	(0.0067, 0.0141)	(0.0034, 0.0074)
HF	(0.0275, 0.0538)	(0.0142, 0.0305)	(0.0070, 0.0154)	(0.0035, 0.0079)
BD	(0.0273, 0.0524)	(0.0137, 0.0280)	(0.0069, 0.0153)	(0.0035, 0.0081)
	(e_2, e_∞)			
DC	(0.0650, 0.2000)	(0.0326, 0.1088)	(0.0163, 0.0490)	(0.0081, 0.0259)
HF	(0.0883, 0.2238)	(0.0418, 0.1405)	(0.0203, 0.1386)	(0.0100, 0.1379)
BD	(0.1333, 0.2028)	(0.0781, 0.1278)	(0.0445, 0.0690)	(0.0277, 0.0344)
	(d_2, d_∞)			
DC	0.096	0.584	3.11	24.5
HF	0.987	3.14	12.0	47.3
BD	19.0	77.8	322	1821
	Timing (sec)			

Planar Region. The main purpose of this example is to show how the quality of the input triangulation affects the conformality. We generate a triangulation with 1500 vertices of a

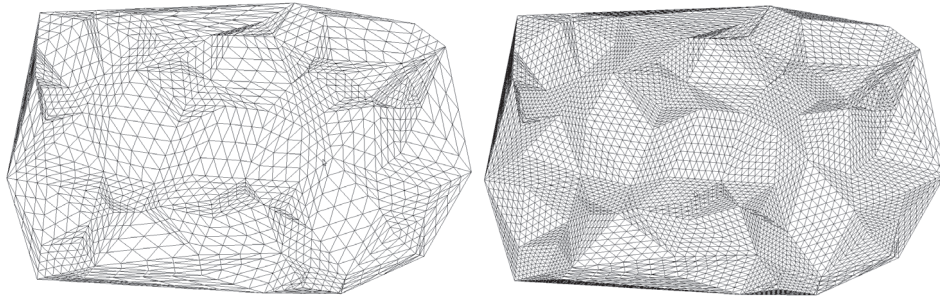


Figure 16. The input triangulations of Planar Region with 1500 vertices (left) and 5000 vertices (right).

Table 3

Planar Region: Approximation errors and running time.

Method	1500	5000	20000	80000
DC	(0.0553, 0.2692)	(0.0286, 0.1292)	(0.0144, 0.0738)	(0.0072, 0.0401)
HF	(0.0881, 0.9840)	(0.0473, 0.5649)	(0.0210, 0.5558)	(0.0093, 0.5570)
BD	(0.1333, 1.307)	(0.0781, 1.285)	(0.0445, 1.482)	(0.0277, 1.324)
(d_2, d_∞)				
DC	0.096	0.584	3.11	24.5
HF	0.987	3.14	12.0	47.3
BD	74.2	227	940	4204
Timing (sec)				

planar region, as shown on the left in Figure 16, and then subdivide the triangulation three times by adding the midpoints of the edges and splitting each triangle into four smaller ones, and finally obtain three more continuously refined triangulations of the planar region with approximately 5000, 20000, and 80000 vertices. The right picture in Figure 16 shows the one with about 5000 vertices. There are a few triangles, in particular near the boundary, having the largest angle close to π .

We run the aforementioned methods over these triangulations. The DC and BD methods map them onto an equilateral triangle, while the HF method maps them onto the unit disk. In this example, we do not have the ground truth and thus only estimate d_2 and d_∞ errors, as shown in Table 3. Note that the errors are estimated over the polygons or triangles with their vertices more than $1/20$ the diameter of the planar region away from the boundary. Figure 17 shows the conformal distortion by different methods from the triangulation with 1500 vertices. As we can see, the DC method converges linearly in both the d_2 and d_∞ errors, and the HF and BD methods only converge in the d_2 error. In the embedding computed by HF, there are some triangles close to the boundary whose orientations get reversed.

Left Hand. The model Left Hand is obtained using 3-dimensional scanning. The original model has 200k vertices, which is simplified using Meshlab [1] to triangulated surfaces with 800, 2500, 10000, and 40000 vertices. See Figure 18 for two of them. Again, the DC and BD methods map these triangulated surfaces onto an equilateral triangle and the HF method maps them onto the unit disk. We estimate the d_2 and d_∞ errors as shown in Table 4. Note that the errors are estimated over the polygons or triangles with their vertices more

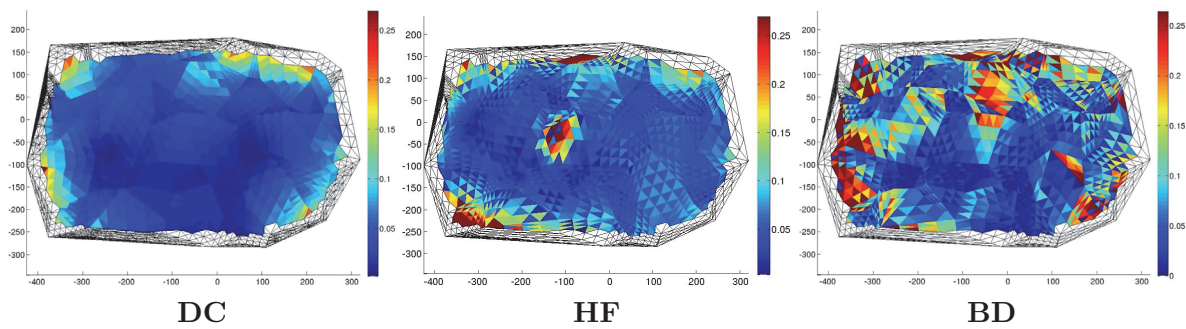


Figure 17. Results for Planar Region: The plots of the conformal distortion $D(h) - 1$ of the planar embedding computed by different methods from the triangulation with 1500 vertices. For purposes of comparison, the range of the color map is fixed at $[0, 0.27]$, although the maximal conformal distortion of the planar embeddings computed by HF and BD is larger than 1.27.

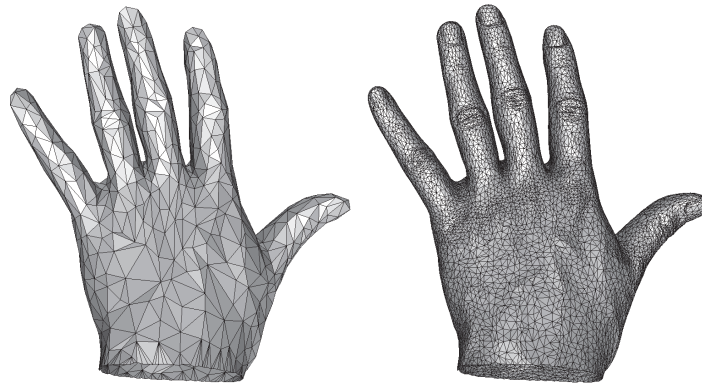


Figure 18. The input triangulation of Left Hand with 800 vertices (left) and 10000 vertices (right).

Table 4

Left Hand: Approximation errors and running time.

Method	800	2500	10000	40000
DC	(0.7436, 2.1873)	(0.3404, 1.1705)	(0.1457, 0.4359)	(0.0686, 0.2651)
HF	(∞, ∞)	(0.4247, 4.0458)	(0.1545, 1.3129)	(0.0716, 2.0045)
BD	(1.1520, 6.5863)	(0.7330, 4.9571)	(0.3930, 3.9686)	(0.2873, 5.2264)
(d_2, d_∞)				
DC	0.236	1.27	5.84	42.3
HF	0.966	2.24	8.52	37.4
BD	38.0	116	475	1941
Timing (sec)				

than $1/60$ the diameter of the planar region away from the boundary. Figure 19 plots the conformal distortions of the planar embedding computed by different methods. For a better visualization, in this example, we show the plots over the planar embedding.

Again the DC method converges linearly in both the d_2 and d_∞ errors, and the HF and BD methods only converge in the d_2 error. In the planar embedding of Left Hand with 800

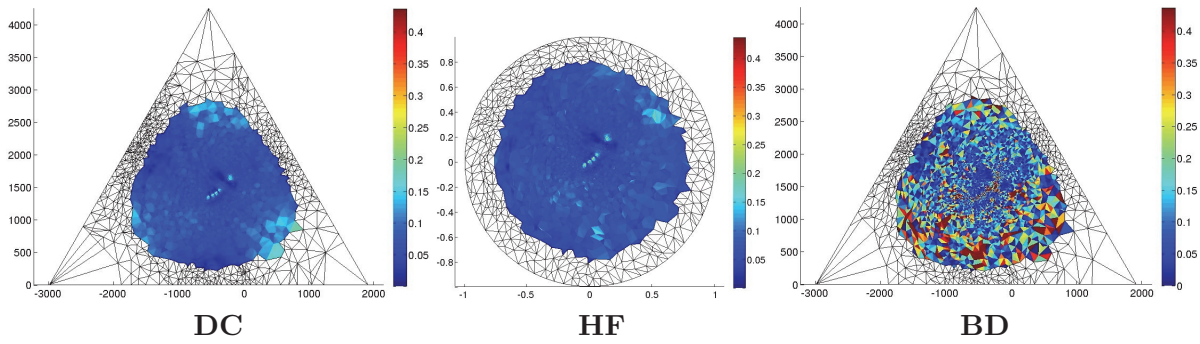


Figure 19. Results for Left Hand: The plots of the conformal distortion $D(h) - 1$ of the planar embedding computed by different methods from the triangulation with 10000 vertices. Note that for purposes of comparison, the range of the color map is fixed at $[0, 0.44]$, although the maximal conformal distortion of the planar embeddings computed by HF and BD is larger than 1.44.

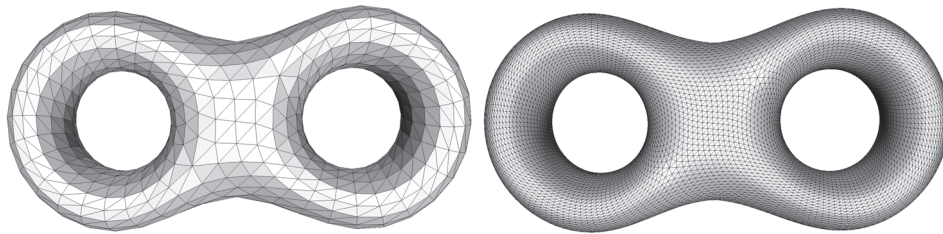


Figure 20. The input triangulations of Eight with 759 vertices (left) and 12000 vertices (right).

Table 5

Eight: Approximation errors and timing.

Method	750	3000	12000	50000	200000
DC	(0.1422, 1.5259)	(0.1112, 0.4187)	(0.0290, 0.2091)	(0.0184, 0.1071)	(0.0085, 0.0361)
HF	(0.1133, 0.3985)	(0.1236, 3.0128)	(0.0828, 6.2417)	(0.0325, 4.7646)	(0.0343, 14.158)
(d_2, d_∞)					
DC	0.040	0.196	1.12	5.88	59.1
HF	1.58	4.91	19.2	80.6	339
Timing (sec)					

vertices computed by the HF method, there are some triangles even away from the boundary whose orientations get reversed. This is the reason the corresponding d_2 and d_∞ errors are ∞ in this case.

Eight. Finally, we check the convergence for different methods over a model called Eight, which is a surface with genus 2. We use Loop subdivision to subdivide a triangulated Eight with about 750 vertices to obtain four more refined triangulated versions of Eight with about 3000, 12000, 50000, and 200000 vertices. Figure 20 shows two of them.

As the implementation of the BD method for surfaces of nondisk topology is not available, we only show the performance of the DC and HF methods. We estimate the d_2 and d_∞ errors as shown in Table 5. Note that the errors are estimated over the polygons or triangles with

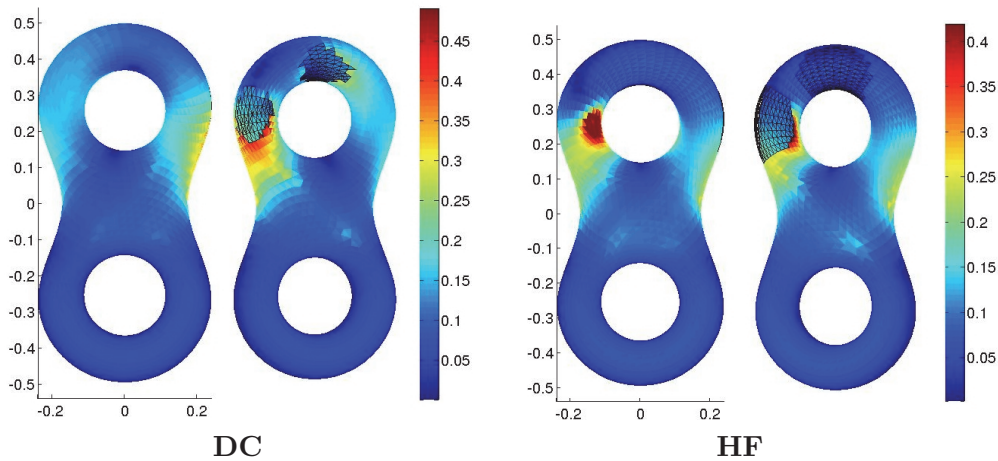


Figure 21. Results for Eight: The conformal distortion $D(h) - 1$ of the planar embedding computed by DC and HF from the triangulation with 3000 vertices plotted on the input surface and shown in two different views. Note that for purposes of comparison, the range of the color map is fixed at $[0, 0.42]$, although the maximal conformal distortion of the planar embeddings computed by HF is larger than 1.42.

their vertices more than $1/20$ the diameter of Eight away from the singular vertices. Again, the DC method converges linearly in both d_2 and d_∞ errors. For the HF method, the d_2 error decreases but the convergence rate is not clear, and the d_∞ error does not even decrease. In this case, the planar embedding is in fact just an immersion and not necessary globally one-to-one. To visualize the conformal distortion, we plot it on the input triangulated surface, as shown in Figure 21.

7.3. More examples and statistics. In this subsection, we present a few more examples and collect a few statistics showing the performance of our algorithm.

We run our DC method on four more examples: Maxplanck (a disk), Brain (a sphere), Protein (a torus), and Genus3 (a 3-hole torus). The results are shown in Figure 22. The d_2 and d_∞ errors are estimated over the polygonal faces whose vertices are more than $1/60$ the diameter of the model away from either the boundary or the singular vertices. Note that there is no singular points for Protein since its Euler characteristic number is 0. For the model Genus3, we only choose one singular vertex.

In Table 6, we collect the following statistics when the algorithm runs over various examples: (1) the number of triangles in the input triangulated surface, labeled $\#Fin$, representing the input complexity; (2) the number of polygonal faces in the common refinement of $T \cup T'$, labeled $\#Fout$, representing the output complexity; for surfaces with boundary, we count half of the faces in $T \cup T'$; (3) the number of diagonal switches needed to transform the input triangulation T_0 to the Delaunay triangulation T , labeled $\#DelSW$; (4) the running time in second of the above diagonal switches, labeled $tDelSW$; (5) the number of cocircular diagonal switches performed during the discrete conformal deformation, labeled $\#CocSW$; (6) the running time in second of the above cocircular diagonal switches, labeled $tCocSW$; (7) the number of the Newton iterations, labeled $\#Newton$; (8) the running time in second of the Newton iterations excluding $tCocSW$, labeled $tNewton$. From Table 6, we observe that the

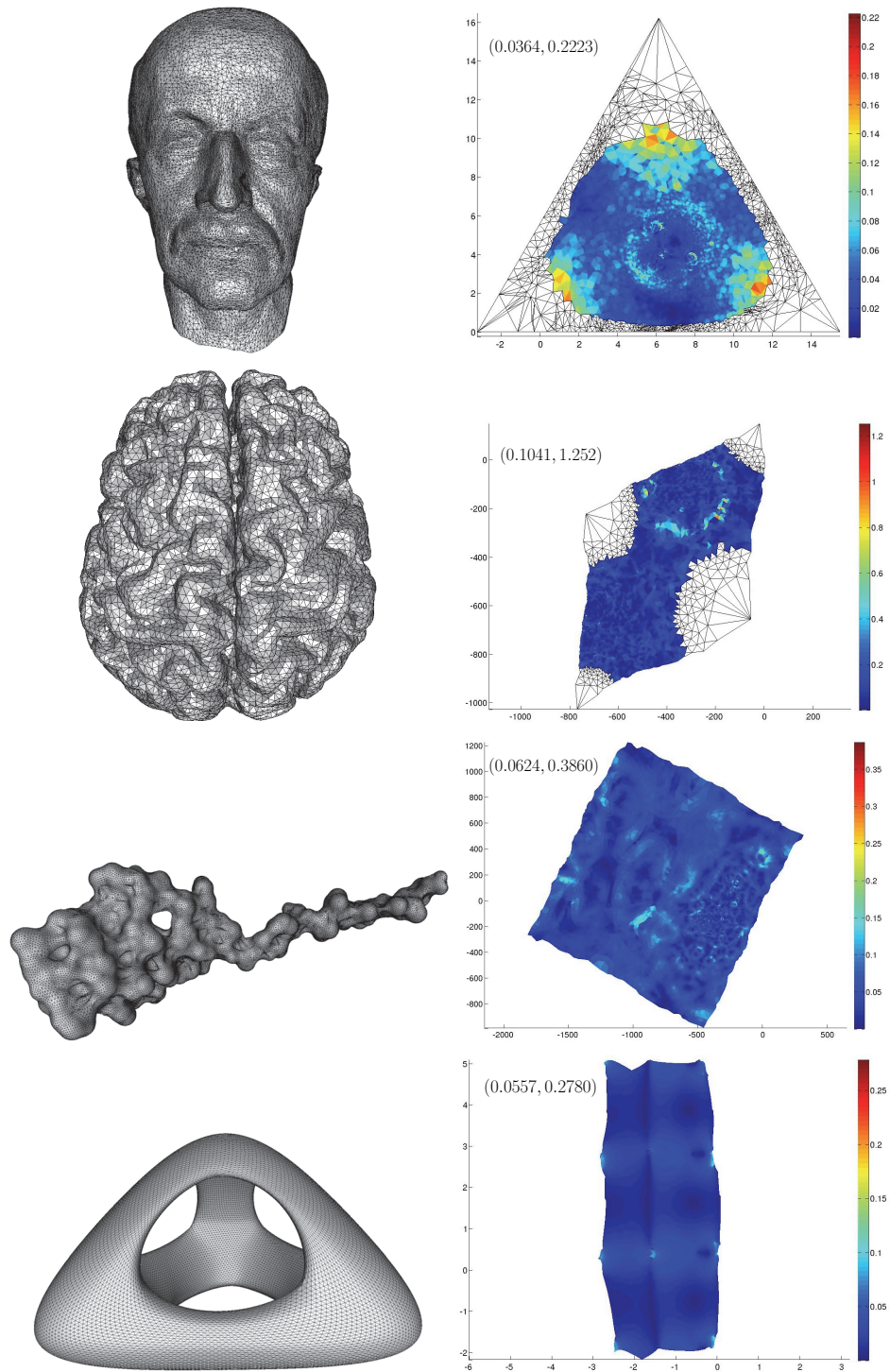


Figure 22. Left: The input triangulated surfaces. Right: The planar embedding computed by our algorithm. The color maps plot $D(h) - 1$, and the pairs of numbers are the (d_2, d_∞) errors.

Table 6
Statistics.

Model	#Fin (k)	#Fout (k)	#DelSW	tDelSW	#CocSW	tCocSW	#Newton	tNewton
Planar Region	10.22	10.25	3223	0.072	14	0.272	5	0.34
Planar Region	40.86	40.90	14113	0.38	17	1.30	5	2.01
Planar Region	163.47	163.50	59288	1.50	18	5.41	5	13.53
Left Hand	79.98	80.54	14192	0.52	272	30.6	7	4.97
Eight	196.61	196.65	68428	0.34	44	13.84	5	43.1
Maxplanck	47.08	47.27	5969	0.248	93	4.53	6	2.22
Brain	15.00	15.30	1048	0.016	300	4.6	6	1.05
Protein	46.24	46.37	3064	0.072	132	8.07	9	5.34
Genus3	26.62	26.74	12454	0.052	111	4.33	10	4.56

number of faces in $T \cup T'$ is often only a few hundred more than that in T , Newton's method converges very fast and takes only 5–10 iterations, and diagonal switch costs very little. Note that the procedure of cocircular diagonal switch takes more time since it must find the first edge failing the Delaunay condition along the deforming path.

7.4. Remark. From the above experiments, we observe that our conformality numerically converges to the classical one as the triangle size goes to 0, at a linear rate. In particular, this convergence behavior is independent of the quality of the triangles in the input triangulated surfaces. It is also very efficient compared to the state of the art. One disadvantage of our method is that we may subdivide the input triangles into the polygonal pieces to accurately represent the discrete conformal map. This may increase the complexity of the output by our algorithm. However, from the statistics we show, the increase of the complexity is very little for most of the prescribed curvatures.

8. Conclusion. We have introduced a new discrete conformality for triangulated surfaces possibly with boundary, showed a discrete uniformization theorem with this conformality, described an algorithm for solving the problem of prescribing curvature, and explicitly constructed a discrete conformal map between the input triangulated surface and the deformed triangulated surface. In addition, we have presented the numerical examples to show the convergence of our discrete conformality and to demonstrate the efficiency and the robustness of our algorithm.

We point out a few possible directions for future research. In [13], we have presented a similar discrete conformality for hyperbolic triangulated surfaces and a discrete uniformization theorem associated to it. We plan to develop an algorithm based on this discrete conformality to solve the problem of prescribing curvature for hyperbolic triangulated surfaces. Hyperbolic triangulation is more natural for surfaces with genus bigger than 1 as their fundamental domains can be flattened into a hyperbolic plane without choosing any singular vertices. It remains open whether our discrete conformality and uniformization theorem can be extended to spherical triangulated surfaces, which is definitely worth investigating in the future. Another interesting avenue for future research is to see whether diagonal switches can be used in inversive distance circle patterns.

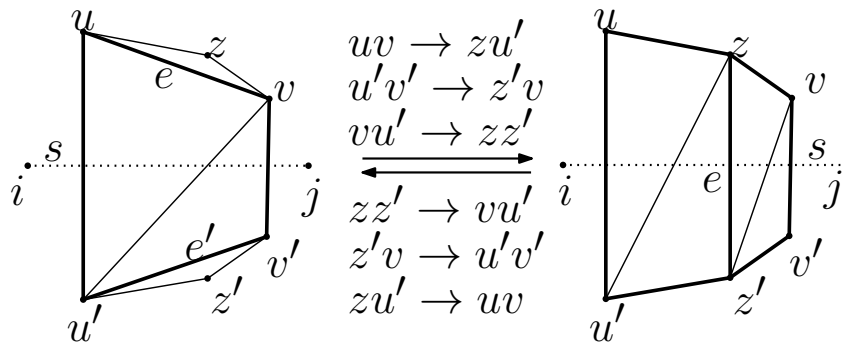


Figure 23. Diagonal switches for the edges of the triangles crossing a segment on the boundary. From left to right: The edges $e = uv, e' = u'v'$ always fail to be Delaunay at the same time. After their switches, the edges $u'v$ fail to be Delaunay. From right to left: The edges $e = zz', zu',$ and vz' always fail to be Delaunay at the same time.

Appendix: Proof of Theorem 3.4.

Proof. Denote by (\tilde{S}, \tilde{V}) the doubled surface of (S, V) and by \tilde{d} the doubled metric of d . Prescribe the curvature \tilde{K}^* for (\tilde{S}, \tilde{V}) by setting $\tilde{K}^*(v) = 2 * K^*(v)$ for a vertex v on the boundary, and $\tilde{K}^*(v) = K^*(v)$ for a vertex v in the interior. It is easy to verify that the curvature \tilde{K}^* satisfies the hypotheses in Theorem 3.2 imposed on a prescribed curvature on (\tilde{S}, \tilde{V}) . Thus there exists a PL metric \tilde{d}' discrete conformal to \tilde{d} , and the discrete curvature of \tilde{d}' is the curvature of \tilde{K}^* . We will show that \tilde{d}' respects the doubling structure and that the restriction of \tilde{d}' onto S is the PL metric d' with the property stated in the theorem.

We first show for a PL metric dd on (\tilde{S}, \tilde{V}) respecting the doubling structure that there is a Delaunay triangulation T in dd which has the following symmetric property: (1) Any triangle f in T not crossing the boundary has an identical mirror triangle $f' = h(f)$ in T . (2) Let $F_s(T)$ be set of triangles in T crossing a segment $s \in B$. Then any triangle $f = uv'v \in F_s(T)$ must have a pair of vertices u, u' with $u' = h(u)$, and moreover, if the third vertex v of f is not the endpoints of the segment s , the neighboring triangle $f' = v'vu' \in F_s(T)$ has the property that $v' = h(v)$. Note that the quadrilateral $f \cup f'$ must be cocircular as the segment s is the common bisector of the edge uu' and vv' . See Figure 4 for an illustration.

Since one can reach a Delaunay triangulation starting from any triangulation by diagonally switching the edges which fail to be Delaunay finite many times, we can prove this by induction on the number of diagonal switches. We start with the triangulation T_0 on (\tilde{S}, \tilde{V}) so that the restrictions of T_0 onto both copies of S are identical triangulations. Note that a segment $s \in B$ must be an edge in T_0 . Thus $F_s(T_0)$ is empty and the symmetric property trivially holds. Assume that by diagonally switching a set of edges which fails to be Delaunay, we reach a triangulation T_k satisfying the symmetric property. Assume there is an edge $e \in T_k$ which fails to be Delaunay. If e is not a side of any triangle in $F_s(T_k)$ for any segment $s \in B$, then its mirror $h(e)$ also fails to be Delaunay. Note that if the edge e itself is a segment on B , then $h(e) = e$. Switch both e and $h(e)$ and reach a triangulation T_{k+1} which satisfies the symmetric property. If e is a side of a triangle in $F_s(T_k)$ for some segment $s \in B$, there are two cases: (i) e crosses s ; and (ii) e does not cross e . In the case (i), the endpoints z, z' of e must satisfy $z' = h(z)$, and any edge in the triangles incident to e which crosses s must also fail to

be Delaunay. For example, as shown in Figure 23, the edges zu' and $z'v$ must also fail to be Delaunay. Switch these edges and reach a triangulation T_{k+1} which satisfies the symmetric property. In the second case, switch both e and $e' = h(e)$. If the endpoints of e contain no endpoints of the segment s , as shown in Figure 23, switch the diagonal vu' , as it must also fail to be Delaunay. The resulting triangulation T_{k+1} satisfies the symmetric property. This proves that there is a Delaunay triangulation T in dd satisfying the above symmetric property.

Let $w : \tilde{V} \rightarrow \tilde{V}$ with $\sum_{v \in \tilde{V}} w(v) = 0$ be the conformal factor such that $\tilde{d}' = w * \tilde{d}$. We claim w respects the doubling structure, i.e., $w(v) = w(h(v))$ for any vertex $v \in \tilde{V}$. Otherwise, let us define a new conformal factor w' so that $w'(v) = w(h(v))$ for any vertex $v \in \tilde{V}$, and then $w' \neq w$, which from Lemma 4.1 implies the metric $w' * \tilde{d}$ is different from \tilde{d}' . However, it is easy to verify that the curvature of the metric $w' * \tilde{d}$ is also equal to \tilde{K}^* . This contradicts the uniqueness of \tilde{d}' .

Now let $w(t) = tw$ for $t \in [0, 1]$ be a path from 0 to w ; we have that $w(t)$ respects the doubling structure for any t . As discussed in section 4, $\tilde{d}(t) = w(t) * \tilde{d}$ for $t \in [0, 1]$ is a path in $C(\tilde{d})$. Let $0 = t_0 < t_1 < t_2 < \dots < t_m = 1$ be a partition of $[0, 1]$ so that for any $0 \leq i \leq m-1$, $\tilde{d}(t)$ with $t \in [t_i, t_{i+1}]$ is a path inside the cell $\mathcal{M}_D(T_i)$ for some triangulation T_i . If $\tilde{d}(t_i)$ respects the doubling structure and T_i satisfies the symmetric property in the metric $\tilde{d}(t_i)$, then T_i remains so in any PL metric $\tilde{d}(t)$ for any $t \in [t_i, t_{i+1}]$. Indeed, the symmetric property (1) obviously holds as $w(t)$ respects the doubling structure. To show the symmetric property (2), it suffices to show that the quadrilateral $f \cup f'$ remains cocircular. This can be done by verifying that the sum of the cosines of the angles opposite to the diagonal remains 0 along the path $w(t)$. Furthermore, consider the region $\cup_{f \in F_s(T_i)} f$, as shown in Figure 4. One can cut it into two geometrically identical subregions using a straight line connecting the endpoints of the segment s and passing through the midpoints of the edges in $F_s(T_i)$ of the form uu' with $u' = h(u)$. This shows that $\tilde{d}(t)$ respects the doubling structure for any $t \in [t_i, t_{i+1}]$; in particular, so does $\tilde{d}(t_{i+1})$. Now by construction, $\tilde{d}(t_0)$ respects the doubling structure. From the previous discussion, $\tilde{d}(t_0)$ lies in the cell $\mathcal{M}_D(T_0)$, where T_0 satisfies the symmetric property. Then, using induction, we show that $\tilde{d}' = \tilde{d}(1)$ respects the double structure. The restriction of \tilde{d}' onto S is the PL metric d' on (S, V) . Finally, it is easy to verify that the curvature on S in d' equals K^* . This proves the theorem. ■

Acknowledgments. We would like to thank Yaron Lipman for the implementation of the BD method, and Xianfeng Gu and S-T. Yau for the implementation of the HF method.

REFERENCES

- [1] *MeshLab*, <http://meshlab.sourceforge.net/>.
- [2] N. AMENTA, S. CHOI, T. K. DEY, AND N. LEEKHA, *A simple algorithm for homeomorphic surface reconstruction*, Internat. J. Comput. Geom. Appl., 12 (2002), pp. 125–141.
- [3] E. D. ANDERSEN AND K. D. ANDERSEN, *The MOSEK interior point optimizer for linear programming: An implementation of the homogeneous algorithm*, in High Performance Optimization, Appl. Optim. 33, H. Frenk, K. Roos, T. Terlaky, and S. Zhang, eds., Springer, New York, 2000, pp. 197–232.
- [4] A. BOBENKO, U. PINKALL, AND B. SPRINGBORN, *Discrete Conformal Maps and Ideal Hyperbolic Polyhedra*, preprint, arXiv:1005.2698, 2010.
- [5] A. BOBENKO AND B. SPRINGBORN, *A discrete Laplace-Beltrami operator for simplicial surfaces*, Discrete Comput. Geom., 38 (2007), pp. 740–756.

- [6] P. L. BOWERS AND K. STEPHENSON, *Uniformizing dessins and Belyĭ maps via circle packing*, Mem. Amer. Math. Soc., 170 (2004).
- [7] B. CHOW AND F. LUO, *Combinatorial Ricci flows on surfaces*, J. Differential Geom., 63 (2003), pp. 97–129.
- [8] Y. COLIN DE VERDIÈRE, *Un principe variationnel pour les empilements de cercles*, Invent. Math., 104 (1991), pp. 655–669.
- [9] T. A. DRISCOLL, *The Schwarz-Christoffel Toolbox for MATLAB*, <http://www.math.udel.edu/~driscoll/SC>.
- [10] M. FISHER, B. SPRINGBORN, A. I. BOBENKO, AND P. SCHRODER, *An algorithm for the construction of intrinsic Delaunay triangulations with applications to digital geometry processing*, in ACM SIGGRAPH 2006 Courses, SIGGRAPH '06, ACM, New York, 2006, pp. 69–74.
- [11] D. GLICKENSTEIN, *A combinatorial Yamabe flow in three dimensions*, Topology, 44 (2005), pp. 791–808.
- [12] D. GLICKENSTEIN, *A maximum principle for combinatorial Yamabe flow*, Topology, 44 (2005), pp. 809–825.
- [13] X. GU, R. GUO, F. LUO, J. SUN, AND T. WU, *A Discrete Uniformization Theorem for Polyhedral Surfaces II*, preprint, arXiv:1401.4594, 2014.
- [14] X. GU, F. LUO, J. SUN, AND T. WU, *Discrete conformal mapping for polyhedral surfaces*, in preparation.
- [15] X. GU, F. LUO, J. SUN, AND T. WU, *A Discrete Uniformization Theorem for Polyhedral Surfaces*, preprint, arXiv:1309.4175, 2013.
- [16] X. GU AND S.-T. YAU, *Global conformal surface parameterization*, in Proceedings of the 2003 Eurographics/ACM SIGGRAPH Symposium on Geometry Processing, SGP '03, Aire-la-Ville, Switzerland, Eurographics Association, 2003, pp. 127–137.
- [17] X. GU AND S.-T. YAU, *Computational Conformal Geometry*, Adv. Lect. Math. 3, International Press of Boston, 2008.
- [18] R. GUO, *Local rigidity of inversive distance circle packing*, Trans. Amer. Math. Soc., 363 (2011), pp. 4757–4776.
- [19] A. HATCHER, *On triangulations of surfaces*, Topology Appl., 40 (1991), pp. 189–194.
- [20] Z.-X. HE AND O. SCHRAMM, *The C^∞ -convergence of hexagonal disk packings to the Riemann map*, Acta Math., 180 (1998), pp. 219–245.
- [21] S. HERSONSKY, *Boundary value problems on planar graphs and flat surfaces with integer cone singularities, I: The Dirichlet problem*, J. Reine Angew. Math., 2012 (2011), pp. 65–92.
- [22] S. HERSONSKY, *Boundary value problems on planar graphs and flat surfaces with integer cone singularities, II: The mixed Dirichlet-Neumann problem*, Differential Geom. Appl., 29 (2011), pp. 329–347.
- [23] S. HERSONSKY, *The triple intersection property, three dimensional extremal length, and tiling of a topological cube*, Topology Appl., 159 (2012), pp. 2795–2805.
- [24] M. JIN, J. KIM, F. LUO, AND X. GU, *Discrete surface Ricci flow*, IEEE Trans. Vis. Comput. Graph., 14 (2008), pp. 1030–1043.
- [25] L. KHAREVYCH, B. SPRINGBORN, AND P. SCHRÖDER, *Discrete conformal mappings via circle patterns*, ACM Trans. Graph., 25 (2006), pp. 412–438.
- [26] B. LÉVY, S. PETITJEAN, N. RAY, AND J. MAILLOT, *Least squares conformal maps for automatic texture atlas generation*, ACM Trans. Graph., 21 (2002), pp. 362–371.
- [27] Y. LIPMAN, *Bounded distortion mapping spaces for triangular meshes*, ACM Trans. Graph., 31 (2012), 108.
- [28] L. M. LUI, K. C. LAM, S.-T. YAU, AND X. GU, *Teichmüller mapping (T -map) and its applications to landmark matching registration*, SIAM J. Imaging Sci., 7 (2014), pp. 391–426.
- [29] F. LUO, *Combinatorial Yamabe flow on surfaces*, Commun. Contemp. Math., 6 (2004), pp. 765–780.
- [30] F. LUO, *Rigidity of polyhedral surfaces, III*, Geom. Topology, 15 (2011), pp. 2299–2319.
- [31] U. PINKALL AND K. POLTHIER, *Computing discrete minimal surfaces and their conjugates*, Experiment. Math., 2 (1993), pp. 15–36.
- [32] I. RIVIN, *Euclidean structures on simplicial surfaces and hyperbolic volume*, Ann. of Math. (2), 139 (1994), pp. 553–580.
- [33] M. ROČEK AND R. M. WILLIAMS, *The quantization of Regge calculus*, Z. Phys. C Particles and Fields, 21 (1984), pp. 371–381.

- [34] B. RODIN AND D. SULLIVAN, *The convergence of circle packings to the Riemann mapping*, J. Differential Geom., 26 (1987), pp. 349–360.
- [35] B. SPRINGBORN, P. SCHRÖDER, AND U. PINKALL, *Conformal equivalence of triangle meshes*, ACM Trans. Graph., 27 (2008), pp. 77:1–77:11.
- [36] K. STEPHENSON, *Circle packing: A mathematical tale*, Notices Amer. Math. Soc., 50 (2003), pp. 1376–1388.